

Magmatic Evolution of the Western Branch of the East African Rift System Melts: Evidence by Silicate Melt Inclusions, Rock Petrography and Geochemistry of the Nyiragongo 1977 and 2002 Lavas in DRC

Douxdoux Kumakele Makutu^{1,2} 

¹Department of Energy Resource Engineering, College of Engineering, Inha University, Incheon, Republic of Korea

²Department of Geosciences, College of Natural Sciences, Kinshasa University, Kinshasa, Republic Democratic of Congo

Email: dx7itaewon@gmail.com

How to cite this paper: Makutu, D.K. (2023) Magmatic Evolution of the Western Branch of the East African Rift System Melts: Evidence by Silicate Melt Inclusions, Rock Petrography and Geochemistry of the Nyiragongo 1977 and 2002 Lavas in DRC. *Open Journal of Geology*, **13**, 449-486.

<https://doi.org/10.4236/ojg.2023.135021>

Received: April 17, 2023

Accepted: May 28, 2023

Published: May 31, 2023

Copyright © 2023 by author(s) and Scientific Research Publishing Inc. This work is licensed under the Creative Commons Attribution International License (CC BY 4.0).

<http://creativecommons.org/licenses/by/4.0/>



Open Access

Abstract

Nyiragongo volcanic eruptions of 1977 and 2002 emitted silica-undersaturated lavas named melilite-nephelinites with microlithic to sub-porphyrific textures, and consisted of olivine, clinopyroxene (augite), phlogopite, melilite, magnetite, and rare plagioclases. This melilite-nephelinite as an evolved rock, shows low SiO₂ (38.40 - 39.52 wt%) and MgO (3.10 - 4.01 wt%), and relatively high FeOt (13.76 - 14.10 wt%), Al₂O₃ (15.01 - 16.48 wt%), CaO (11.00 - 12.29 wt%) and Na₂O + K₂O (10.34 - 11.85 wt%). Unlike LA-ICP-MS on silicate melt inclusions (SMIs) hosted in augite show a pristine melt of microbasaltic (low Ti-picrite) rock poor in SiO₂ (31.14 - 32.26 wt%), FeOt (2.19 - 2.79 wt%), Al₂O₃ (8.01 - 9.57 wt%), and Na₂O + K₂O (2.34 - 3.05 wt%), while enriched in MgO (20.27 - 28.63 wt%), and CaO (24.95 - 33.17 wt%). The sums (Σ REEs) for lavas and SMIs are ranging 712 - 799 and 43 - 119 ppm respectively. REE contracted multi-element patterns showed a W-feature for most lavas except for SMIs. High Rb/Sr, and low Ba/Rb, Zr/Nb, and Sm/Hf ratios of lavas suggest a phlogopite-rich source of materials.

Keywords

Nyiragongo Lava, Petrography, Geochemistry, SMIs, LA-ICP-MS, Rifting, Magma Evolution

1. Introduction

The East African Rift System (EARS) affects the eastern part of the African con-

continent where about 10 counties even more are concerned, starting from Ethiopia-Djibouti in the North until Mozambique-Malawi in the South. This rift is subdivided into Eastern and Western branches [1] [2] [3]. The Eastern branch (EB) crosscuts countries including Djibouti, Ethiopia, Kenya, Tanzania, Malawi, and Mozambique, while the Western branch (WB) includes countries such as Uganda, Democratic Republic of the Congo, Rwanda, and Burundi. The WB is geographically subdivided into three main volcanic provinces that include from the North to South, the Toro-Ankole volcanic field (T.A.V.F.), Virunga volcanic field (V.V.F.) and Kivu South volcanic field (K.V.F.), (Figure 1), [4] [5] [6] [7]

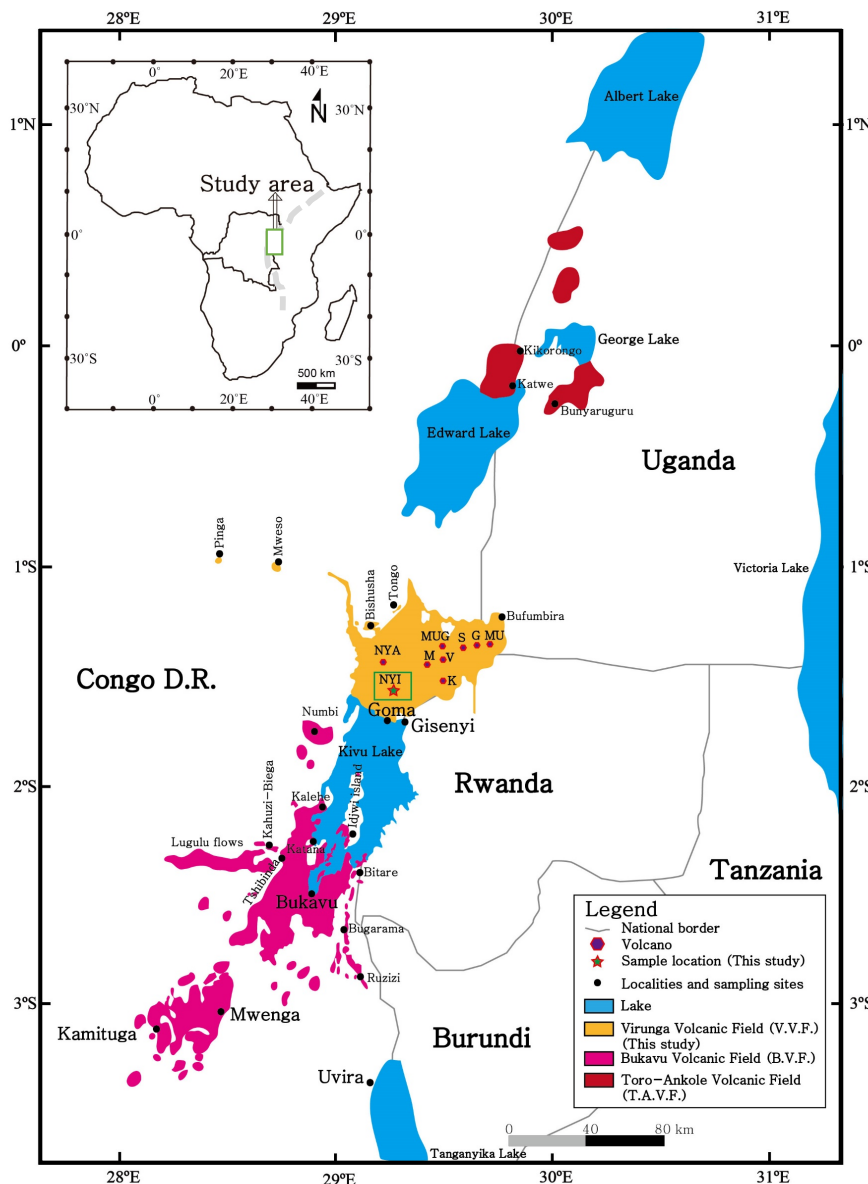


Figure 1. A simplified map showing several volcanic rock fields in the western branch of the East African Rift System in Congo D.R., Uganda, and Rwanda. The green rectangle is used for the study area. (For Virunga field volcanoes: NYA = Nyamuragira, NYI = Nyiragongo, M = Mikeno, K = Karisimbi, V = Visoke, MUG = Mugogo, S = Sabinyo, G = Gahinga, MU = Muhavura). Modified after [1] [6].

[8]. The WB hosts numeral lakes such as Albert, Edward, George, Kivu, Tanganyika, and Mweru (**Figure 1, Figure 2**).

The Nyiragongo volcano is part of the Virunga Volcanic Province that hosts from East to West, about 9 main stratovolcanoes including large Muhavura (4127 m), Gahinga (2474 m), Sabinyo (3647 m), Visoke (3711 m), Karisimbi (4507 m), Mugogo (4230 m), Mikeno (4437 m), Nyiragongo (3470 m), and finally the large shield volcano Nyamuragira (3058 m); and hundreds minor centers have been documented (**Figure 2**), [6] [9] [10] [11]. The Nyiragongo and Nyamuragira are two most active volcanoes in the WB of the EARS and classified as two of hundred dangerous active volcanoes in the world by the International Association of Volcanology and Chemistry on Earth's Interior (IAVCEI) in the early 20th century [12] [13] [14] [15].

The Nyiragongo stratovolcano is well known for exhibiting a permanent lava lake on its crater, and shows features such as a well-structured plumbing system of the edifice that makes this volcano unique in the world [16] [17] [18]. The emitted lavas from the mount Nyiragongo are highly fluidized buoyant flows and consist of alkali basalts, leucite nephelinite, melilite nephelinite and olivine melilitite [4] [6] [11] [18]-[24].

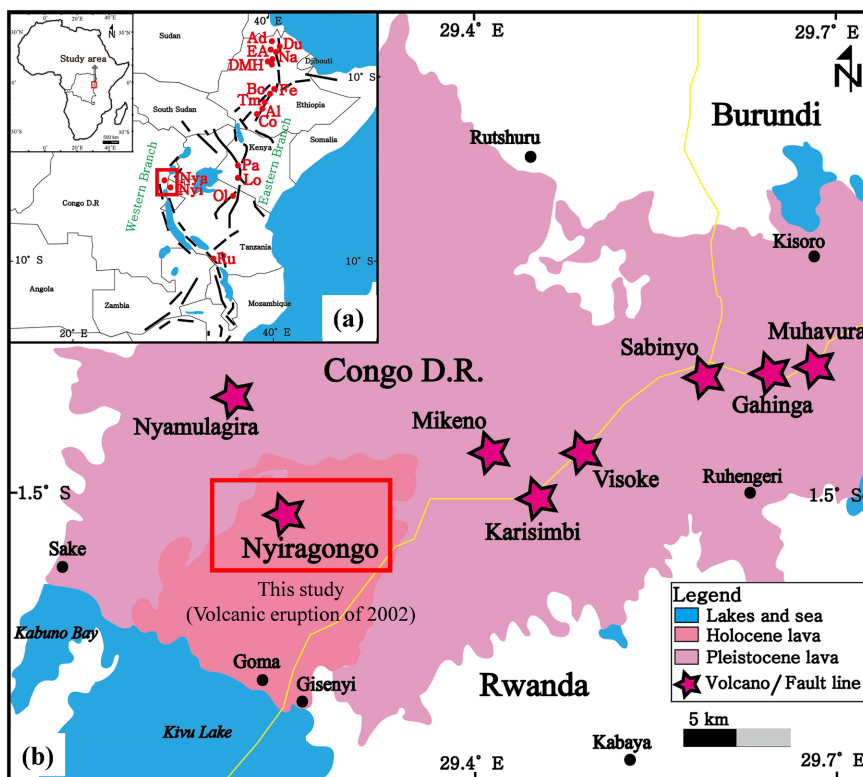


Figure 2. (a) A simplified map of volcano distributions in Africa especially in the East African Rift System including Erte Ale (EA), Alu-Dalafilla (Ad), Dubbi (Du), Nabro (Na), Dabbahu Manda Hararo (DMH), Fentale (Fe), Boset (Bo), Tullu Moye (Tm), Aluto (Al), Corbetti (Co), Paka (Pa), Longonot (Lo), Oldoinyo Lengai (OL), Nyamuragira (Nya), Nyiragongo (Nyi), and Rungwe (Ru); (b) Distribution of volcanoes in the Virunga volcanic field (V.V.F.) in the DRC. The red rectangles show the study area. Modified after [3].

The Nyiragongo started its volcanic activities approximately 12 ka ago, and in the 21st century, few eruptions were the most important and recent eruptions are of January 2002, July 2012 and June 2021 with considerable human and material damages [6] [7] [11] [25] [26] [27].

This study establishes a connection of silica melt inclusion petrochemistry with petrographic and geochemical characteristics of the Nyiragongo 1977 and 2002 lavas, and other historical data in order to constrain magmatic and morphological evolutions of the rifting. This study also provides petrographic, morphological and geochemical specificities of the Nyiragongo volcano compared to other active and dormant volcanoes of the Virunga Volcanic Field (VVF) in particular, and worldwide known volcanoes in general.

This study mainly aims 1) to compare mineralogical and geochemical compositions of historical lava data with those obtained in this research (1977 and 2002 lavas); 2) connect petrographic and geochemical results of silicate melt inclusions trapped in deep zones with those of the surface lavas in order to possibly detect any similarities and discrepancies; 3) identify the petrochemical proxies that better characterize the magmatic evolution in the western branch of the EARS from the initially formed magmas by the melting of the mantle wedge to evolved and differentiated melts in subsurface magmatic chambers.

2. Geological Background

2.1. The East African Rifting Framework, Volcanic Activities, and Rock Petrogenesis

A rifting is a naturally occurring process in the earth's surface and consists of the separation or breaking of the crust through faulting that is caused by the plate tectonic movements. The East African Rift System is a classic example of rifting framework, and crosscut the relatively stable continent of Africa in its eastern zones starting from Djibouti-Ethiopia to Malawi-Mozambique [1] [2] [3] [28]. This EARS extends over 2000 km from the Red Sea in the north to Mozambique in the south and traverses two regions of topographic uplift, the Ethiopian dome in the north and the Kenyan dome in the south, separated by the Turkana depression, the Anza graben and several micro-grabens resulting from trans compressional and transtensional constraints [4] [25] [29] [30]. The EARS is subdivided into eastern and western branches; and it is geomorphologically and spatially characterized by an alignment of volcanoes and lakes (**Figure 1**), [2] [3] [6] [7] [21] [22]. The western branch (WB) is bordered and crosscut by great lineaments, faults, and multiple gashes of variable directional trends of such as N-S, NE-SW, and NW-SE; and reshape the zone in grabens, rift valleys and horsts [6] [31]. This WB is spatially subdivided into three volcanic fields including towards north to south the Toro-Ankole volcanic field (T.A.V.F.), Virunga volcanic field (V.V.F.) and South Kivu volcanic field (K.V.F.) [1] [2] [3] [4] [5] [23] [32] [33].

Volcanic rocks are assigned into three groups according to the area where 1) tholeiites and sodic alkali basalts in the South Kivu, 2) sodic basalts and nepheli-

nites in the northern Lake Kivu and western Virunga, and 3) potassic basanites and potassic nephelinites in the Virunga area [2] [6] [7] [11] [18] [32] [34]. The South-Kivu area magmas are suggested to be generated by the melting of spinel and garnet lherzolite from mixed sources (asthenosphere and lithosphere), the sodic nephelinites of the northern Lake Kivu area are originated from the low partial melting of garnet peridotite of the sub-continental mantle due to pressure release during initiation swelling, and the Virunga potassic magmas were generated during the melting of garnet peridotite (with an increasing degree of melting from nephelinite to basanite) from a lithospheric source enriched in both K and Rb; and therefore, suggest the presence of phlogopite in source materials, and the local existence of a metasomatized mantle and finally the carbonatite contribution as evidenced in the Nyiragongo lavas [4] [5] [6] [11] [18] [20] [34] [35].

In the western branch of the EARS, new K-Ar and Ar-Ar age data showed that the earliest volcanic activity started during the mid-Cenozoic 21 Ma ago and petrographically constituted of nephelinites, then followed by a sodic alkaline volcanism between 13 and 9 Ma at the western side of the Virunga field during the doming stage of the rift and pre-rift valley formation period [6] [7] [23] [34]. In the South-Kivu area, the first 11 Ma dated lavas were tholeiitic and followed at 8 Ma by intensive fracturation and the rift valley subsidence; and the petrographic compositions shifted progressively from tholeiitic to alkali basaltic lavas until the early Quaternary (1.7 Ma) where the renewal of the basaltic volcanism at the western side of the rift [6] [23] [34]. However, the potassic volcanism in the Virunga zone occurred at the end of Cenozoic (2.6 Ma) along a NE-SW fault zone and then migrated both to the east and west, in jumping to oblique tension gashes or lineaments [6] [34].

The magmatic evolution and the high diversity of volcanic rocks of the EARS western branch would be explained by varying transtensional constraints during the rift history, the type and quality of bedrock and weekly by the depth and source of the magma [6] [7] [23] [32].

The Virunga volcanic field hosts two main active volcanoes including Nyamuragira and Nyiragongo, and numeral dormant volcanoes such as Karisimbi, Visoke, Mugogo, Sabinyo, Gahinga, Muhavura and tens of small non-identified volcanic edifices (**Figure 2**) [4] [7] [11] [18] [36]. The Nyiragongo and Nyamuragira volcanoes offer petrographic and geochemical signatures that are representative and summarize well the rift genesis and its evolutive processes [11] [18].

The Nyiragongo volcano is an oxidizing environment, CO₂ rich source deep of 35 km, and ultra-carbonate melt rich is deep of more than 670 km; and Nd-Sm, Rb-Sr, He, U-Pb and Th isotopes suggested an heterogenous source of magma between MORB and enriched mantle beneath the Tanzanian block [4] [5] [6]. A petrographic and geochemical comparisons between Nyiragongo and Nyamuragira revealed that the former is a feldspathoid-k feldspar-plagioclase

(FAP) trend and petrographically consists of basanite and nephelinites whereas the last is a quartz-k feldspar-plagioclase (QAP) trend and hosts a series of volcanic rocks including basalt tholeiites, basanites, hawaiites, mugearites, benmoreites and trachytes [4] [5] [6] [11] [18] [20] [22] [23]. The Nyiragongo lavas show lower Zr/Nb of 1.2 - 2.1 compared to Nyamuragira lavas as of 3.3 - 4.1; $^{87}\text{Sr}/^{86}\text{Sr}$ ratios are 0.7052 - 0.7059 at Nyamuragira while 0.7045 - 0.7047 at Nyiragongo, $^{206}\text{Pb}/^{204}\text{Pb}$ ratios are 19.19 - 19.31 at Nyamuragira while 19.41 - 19.75 at Nyiragongo, and concentrations of Nb (>200 ppm) and S (>500 ppm) are relatively higher at Nyiragongo than Nyamuragira which enriched in halogens such as Cl [4] [11] [18] [36].

2.2. The Kivu Rift Volcanoes, Geometry, Volcanic Eruption Records, and Damages

Nyiragongo and Nyamuragira are among the most active volcanoes in Africa; and they both similarly started volcanic activities about 12 ka ago [7] [11].

Since 1882, The Nyamuragira produced at least 44 eruptions (summit and lateral), offering a dense historical record for that time period [37]. From 1901 to 2012, the Nyamuragira volcano have emitted a volume of magma per summit or flank eruption of $1 - 202 \times 10^6 \text{ m}^3$ and the approximated total volume is estimated at $2445 \times 10^6 \text{ m}^3$ for the period of 19th to 20th century; and averages of $21 - 34 \times 10^6 \text{ m}^3$ per year for the 1901-1940 period, $8 - 16 \times 10^6 \text{ m}^3$ per year for 1940-1980 period, and $26 - 47 \times 10^6 \text{ m}^3$ per year for 1980-2014 period [37] [38] [39].

The Nyiragongo volcanic edifice is a stratovolcano, height of 3470 m, and a relatively circular crater (1 - 2 km of diameter), deep of 395 m and connected to the source at 35 km, with three levels of platform referred as P1 (>3270 m), P2 (>3190 m) and P3 (3075 m and below), where the latter being the active platform that delimits the pit of the permanent and spectacular lava lake and the volcanic system itself is composed of two main parasitic cone such as Baruta in the northern side and Shaheru in the south whereas the Nyamuragira is a large shield stratovolcano height of 3058 m and asymmetrically sub-circular with big axis N-S of 580 m of diameter and small axis E-W of 420 m of diameter [9] [16] [17] [25] [37] [40]. Since 1894, the Nyiragongo crater was known for its semi-permanent active lava lake which levels varied inside inner pits; and these continuous variations of the crater lake level were associated to the internal evolution of the volcanic activities and caused major lateral eruptions on January 10, 1977 [16]. The 1977 eruption was followed by an almost complete collapse of the crater and the active lava lake re-appeared shortly in 1982 and then in 1994; it continuously raised inside the crater and led to the January 17th 2002 volcanic eruption and the following eruptions until June 2021 [9] [11] [16] [18] [27] [41]. The appearance and disappearance of the crater lake is interpreted as a premonitory sign of new venues of the magma and volcanic eruption, which since 1882 until today, the Nyiragongo volcano hosted a record of about 34 volcanic

eruptions [16] [27]. The January 10th 1977 eruption of the Mt. Nyiragongo started by a crater walls fracturation and the lava lake drained the flanks of the edifice in less than 1 hour, with a magma speed of about 60 km/h towards the Goma city [16] [26] [27].

The January 17th 2002 eruption of the Mt. Nyiragongo volcano emitted an estimated volume of $25 - 30 \times 10^6 \text{ m}^3$ of lava [9]. Rheologic properties of the magma after laboratory measurements showed that the viscosity evolution during cooling and crystallization from both 1977 and 2002 eruptions was about 33 Pa s at the liquidus temperature of 1220°C, and was similarly equal to Hawaiian basalts and the lavas remained fluid above 75°C [25]. However, the melt viscosity was approximately 40 Pa s at the liquidus temperature around 1260°C for Nyamuragira lavas, and remains fluid over 110°C [25] [42] [43]. This January 2002 eruption of the Mount Nyiragongo emitted fooidic lavas that covered the southern volcano flank towards the Goma city with velocities of 0.1 - 1 km/h and devastating vast urban areas [19] [25]. Lava flows of Nyiragongo 2002 eruption threaten the city of Goma (pop. ~900,000) and surrounding villages (Sake, etc.), and forcing the rapid exodus of 300,000 to 400,000 people, most of them into Rwanda; hampering the Goma airport and few vents reached the Kivu Lake by forming a small lava delta of about 0.048 km², adding about 35,000 to 70,000 m³ of lava into the lake [9] [25] [26] [27]. About 15% of the surface of the town was affected, causing damages of the business centres and the housing of an estimated 120,000 people, and about 70 to 100 people died directly of eruption, including approximately 30 to 60 collateral deaths from indirect causes such as earthquakes, explosion of a gas station in town, gun shots probably linked to looting [9] [25] [26] [27] [44] [45]. The volcanic eruption of Nyiragongo 1977 did not reach the Goma but was also catastrophic with extremely fast-moving (about 17 m/s) fluid magma that drained and decimated surrounding villages, and killed about 70 persons [9] [25] [26] [27].

The Nyiragongo 1977 and 2002 volcanic eruptions have shown similar chemical, physical and morphological precursory signs as the Kilauea 2018 eruption wherein a significant long-lasting (one-month) fluctuation of SO₂ emissions (estimated from space) and intensive seismic records due to sudden and large drops of the lava lake level associated with strong degassing [45] [46]. On 24 October 2002, a M_w 6.2 earthquake magnitude occurred in the central part of the Lake Kivu basin, Western Branch of the East African Rift and this was the largest event recorded in the Lake Kivu area since 1900 [15] [45]. The composition and flux of gas emitted from Nyiragongo volcano by ground-based remote-sensing techniques and ultraviolet spectroscopic measurements in 2005-2006 indicated average SO₂ emission rates of 23 - 38 kg/s; and the open-path Fourier transform infrared spectroscopic measurements in 2005-2007 reported the presence of water various gas species such as H₂O, CO₂, SO₂, CO, HCl, HF, and OCS (carbonyl sulfide); which average molar proportions are 70, 24, 4.6, 0.87, 0.26, 0.11, and 0.0016% respectively [40] [45]. Additionally, the Nyiragongo volcano have been

responsible of local acid rains of low potential hydrogen (pH: 2 - 4), and wherein significant amounts of harmful components such as SO₂, HCl, HF were detected in the rain waters [41].

3. Methods and Materials

3.1. Identification Methods (Laser Raman, XRD and SEM-EDS)

Raman spectra were acquired using HORIBA HR evolution Raman spectrometer (Inha University, Korea). A calibrated 532 nm laser with 0.8 mW was used for the excitation source, and 30 to 60 seconds of acquisition time. Outcoming signals were processed via Opus and sigma plot software. Raman shift peak positions were used to identify mineral phases.

X-ray diffractometry (XRD) was performed on the bulk-rock (Inha University, Korea), and the amount of 15 - 30 g of the rock powder were thoroughly settled in standard cylindrical sample holders (10 mm of diameter, 2.5 mm of thickness). A diffractometer system XPERT-PRO at a flat stage configuration, where a sample stage was PW3071/xxBracket, and using Cu as anode material. A scanning axis goniometer PW3050 (Theta/Theta), with a minimum step size 2θ of 0.001 and minimum step size ω of 0.001 was used. The apparatus used an accelerating energy of 45 kV and 40 mA of generator voltage. A total of 3237 points have been scanned by using continuous type, and for a time per step of 126.99 s; and the analyzed samples covered a two-theta angle (2θ) ranging 10 - 90 degrees. The outcoming signals were processed via Origin Lab and Sigma Plots software.

Scanning electron microscope energy dispersive spectrometer (SEM-EDS; HR-SEM SU8010 series, Hi-Tech Instruments, Nanjing, China) was performed on augite phenocrysts in Korea (Inha and Busan National University) for getting backscattered images showing zonation features.

3.2. Quantification Methods (EPMA, XRF and LA ICP MS)

Field emission-electron probe micro analyzer (FE-EPMA, JEOL Ltd., Tokyo, Japan) was performed on minerals such as augite, magnetite, microlite and glassy matrix at Busan National University in the Republic of Korea. The electron probe microscope consisted of JEOL-JXA-8530F PLUS model, and used an acceleration voltage of 15 kV, an acceleration current of 10 nA, and an electron beam of 3 mm. The analysis was conducted with a peak duration of 10 s and a background time of 5 s. A non-exhaustive list of analyzed elements included Fe, Mn, Si, Al, K, Ca, Ti, Cr, Na, Mg, Ni, and corresponding standards are hematite (Fe, LIF, $K\alpha$), rutile (Ti, PET, $K\alpha$), pyrope garnet (Mg, TAP, $K\alpha$), spessartine garnet (Mn, LIF, $K\alpha$), corundum (Al, TAP, $K\alpha$), chromite (Cr, PET, $K\alpha$), wollastonite (Si, TAP, $K\alpha$), NiO (Ni, LIF, $K\alpha$) and wollastonite (Ca, PET, $K\alpha$), albite (Na, TAP, $K\alpha$), and biotite (K, PET, $L\alpha$). Outcoming results of major elements were expressed percentage of oxides (wt%).

X-ray fluorescence (XRF, Malvern products, Cambridge, United Kingdom)

was performed on the whole-rock samples at Activation Laboratories-Actlabs in Canada, and signals were acquired based on intensities of pre-selected elements including Si, K, Ca, Na, Ti, Mn, Fe, Mg, Al, and P, as major constituents of silicate minerals in volcanic rocks.

LA-ICP-MS was performed on the bulk-rock lava (at Activation Laboratories-Actlabs, Canada) and on silicate melt inclusions and glassy matrix (at Korea Institute of Ocean Science & Technology-KIOST, Korea). We analyzed 60 isotopes in total (^7Li , ^9Be , ^{23}Na , ^{25}Mg , ^{27}Al , ^{29}Si , ^{39}K , ^{42}Ca , ^{45}Sc , ^{49}Ti , ^{51}V , ^{53}Cr , ^{55}Mn , ^{57}Fe , ^{59}Co , ^{61}Ni , ^{65}Cu , ^{66}Zn , ^{71}Ga , ^{73}Ge , ^{75}As , ^{85}Rb , ^{88}Sr , ^{89}Y , ^{90}Zr , ^{93}Nb , ^{95}Mo , ^{107}Ag , ^{111}Cd , ^{113}In , ^{118}Sn , ^{121}Sb , ^{133}Cs , ^{137}Ba , ^{139}La , ^{140}Ce , ^{141}Pr , ^{146}Nd , ^{147}Sm , ^{151}Eu , ^{157}Gd , ^{159}Tb , ^{163}Dy , ^{165}Ho , ^{167}Er , ^{169}Tm , ^{173}Yb , ^{175}Lu , ^{178}Hf , ^{181}Ta , ^{182}W , ^{185}Re , ^{197}Au , ^{205}Tl , ^{208}Pb , ^{209}Bi , ^{232}Th , ^{238}U); and for glassy matrix and silicate melt inclusions (SMIs), an approximated average of 40 isotopes were consistently detected. For the analysis of SMIs and glassy matrix, a 193 nm Argon-Excimer laser (LA-NWR 193) coupled with a quadrupole mass spectrometer Agilent 7700X (Agilent Technologies, Santa Clara, USA) were used and the ablation was driven in 10 - 12 spots in a raw cycle inset that includes standard reference materials (SRM), with a repetition of 5 Hz, a penetration up to 4 mm and a laser fluency of 3.5 - 6.0 J/cm²; the laser beam diameter of the ablated zone was 30 μm especially for the selected big melt inclusions (>30 μm). A single analysis consisted of 50 seconds of laser dwelling washout, 50 seconds ablation integration with the laser firing and 10 seconds delays before moving to another spot. The mounted sample beads were co-loaded with worldwide reference glasses (NIST-612, BCR-2G) as external standards and Al, Mg and Si were used case by case as internal standards for SMI and glassy matrix respectively. The use of NIST-612 and BCR-2G helped to correct and adjust oxide interferences. Obtained results were processed under the SILLS software where we could distinctly toggle views of signals of both melt inclusion and hosting mineral.

Nevertheless, the present LA-ICPMS analyses of glassy matrix in general, and silicate melt inclusions showed a good reproducibility (90% - 98%) and reliability despite few difficulties in managing the size and the exact volume of the melt inclusion to be ablated. The precision was estimated through repeated analyses of standards, with a relative $1\sigma = 2\% - 10\%$ for the above selected elemental isotopes. An illustration of interpreted signals and results of analyses are provided in this study (**Figure 3; Tables 1-3**).

3.3. Sample Preparations and Descriptions

A total of 7 rock samples (3 for 1977 and 4 for 2002 lavas) were carefully selected, crushed, and milled for various chemical analyses. About 10 thin and 4 polished sections were described under the polarizing microscope (Nikon, Nikon Instruments Inc., New York, NY, USA) at Inha University for mineral phase identifications. About 10 phenocrysts of clinopyroxene (augite) sizing up to 1 cm were selected, and only 2 hosting silicate melt inclusions were located, fully mapped, and targeted for laser ablations.

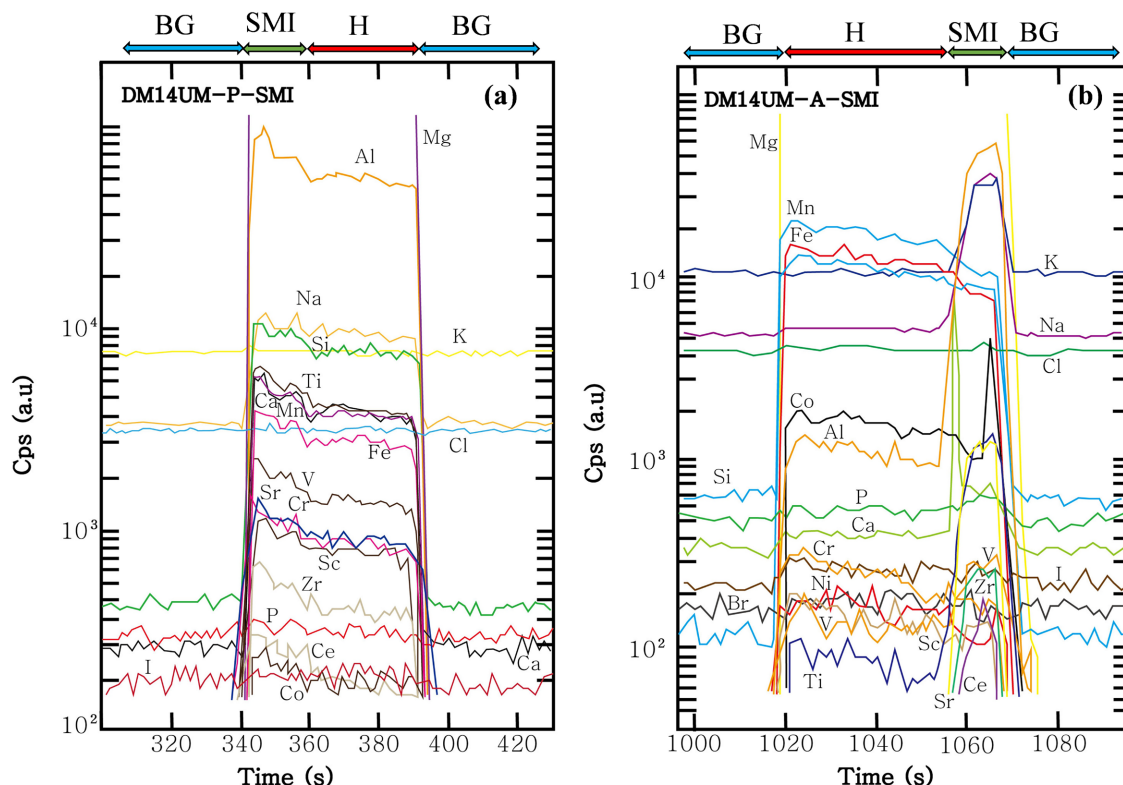


Figure 3. Representative LA-ICP-MS signals of detected silicate melt inclusions: (a) Partially quenched melt inclusion P and (b) partially quenched melt inclusion A. Arrows are used to show the interpreted signal timing ranges and the corresponding material. (BG = background in blue filled arrow, SMI = silicate melt inclusion in green filled arrow, H = hosting mineral in red filled arrow).

Table 1. The whole-rock chemical analyses (XRF and LA ICP MS) of Nyiragongo 1977 and 2002 lavas.

Chemical analyses of Nyiragongo lavas							
Geodynamic context:	Rift						
Rift zone:	East African Rift System						
Rift zone target:	Western Branch (WB)						
Locality:	Goma (North Kivu)/DRC						
Volcano:	Nyiragongo						
Volcano type:	Stratovolcano						
Samples	DM 14UM -Nyira. 2002-1	DM 14UM -Nyira. 1977-1	DM 14UM -Nyira. 2002-2	DM 14UM -Nyira. 1977-2	DM 14UM -Nyira. 2002-3	DM 14UM -Nyira. 1977-3	DM 14UM -Nyira. 2002-4
Major elements							
SiO ₂ (wt%)	38.4	38.6	39	38.5	38.7	38.4	39.5
Al ₂ O ₃ (wt%)	16.5	16.2	16.2	16.5	16.2	16.2	15
FeOt (wt%)	14.1	14	14	14.1	13.8	14.1	13.8
MnO (wt%)	0.2	0.2	0.2	0.1	0.2	0.1	0.3

Continued

MgO (wt%)	3.1	3	3.2	3	3	3	4
K ₂ O (wt%)	5.5	5.5	5.2	5.4	5.6	5.8	5.3
CaO (wt%)	11.1	11	11.2	11.1	11	11.7	12.3
TiO ₂ (wt%)	2.1	2	1.6	1.8	2.1	1.8	1.9
Na ₂ O (wt%)	6	6	6	6.1	6	6.1	5
P ₂ O ₅ (wt%)	1.5	1.6	1.6	1.6	1.6	1.5	1.7
H ₂ O (wt%)	1.5	1.5	1.4	1.4	1.6	1	1
Total (wt%)	100.0	99.6	99.6	99.6	99.8	99.7	99.8
Na ₂ O + K ₂ O (wt%)	11.5	11.5	11.2	11.5	11.6	11.9	10.3
Na ₂ O/K ₂ O	1.1	1.1	1.2	1.1	1.1	1.1	0.9
Mg# [Mg/(Mg + Fe)]	0.2	0.2	0.2	0.2	0.2	0.2	0.2
Minor elements							
Ni (ppm)	40	42	48	45	42	50	40
Sn (ppm)	1	2	2	1	2	2	1
Sc (ppm)	4	4	4	4	4	4	4
Be (ppm)	3	3	3	3	3	3	3
V (ppm)	450	402	355	303	505	313	309
Ba (ppm)	2002	1989	2120	2049	1999	2103	2157
Sr (ppm)	2615	2357	2500	2480	2090	2398	2502
Cr (ppm)	20	15	17	16	19	21	20
Zr (ppm)	351	340	339	401	299	322	345
Co (ppm)	22	38	33	45	40	29	41
Cu (ppm)	203	211	175	169	191	185	180
Zn (ppm)	245	203	148	122	195	205	130
Ga (ppm)	11	15	21	28	16	24	19
Ge (ppm)	1	8	1	2	1	1	1
As (ppm)	4	1	1	2	4	5	5
Rb (ppm)	99	88	89	108	122	106	124
Nb (ppm)	199	218	160	201	180	211	202
Mo (ppm)	1	1	3	2	5	1	4
Ag (ppm)	1	1	1	2	1	1	1
In (ppm)	0	0	0	0	0	0	0
Sb (ppm)	1	0	0	1	0	0	1
Cs (ppm)	1	1	2	1	1	1	1
Hf (ppm)	4	4	5	4	5	5	4
Ta (ppm)	10	13	16	13	14	12	13
W (ppm)	1	2	1	2	1	1	1
Tl (ppm)	0	0	0	0	0	0	0

Continued

Pb (ppm)	6	7	5	6	6	7	5
Bi (ppm)	0	0	0	1	0	0	0
Th (ppm)	22	20	18	20	15	17	18
U (ppm)	7	7	5	4	5	7	6
La (ppm)	182	195	166	180	168	195	182
Ce (ppm)	355	361	341	401	323	399	344
Pr (ppm)	30	35	34	37	35	31	36
Nd (ppm)	128	133	121	122	128	125	125
Sm (ppm)	15	13	18	19	22	13	18
Eu (ppm)	6	7	5	6	6	6	5
Gd (ppm)	10	11	10	12	12	12	11
Tb (ppm)	1	1	1	1	2	2	2
Dy (ppm)	6	7	8	9	8	8	8
Ho (ppm)	1	1	2	2	1	2	1
Er (ppm)	3	3	4	4	4	4	4
Tm (ppm)	0	0	1	0	1	1	1
Yb (ppm)	3	3	3	2	3	3	3
Lu (ppm)	0	0	0	0	0	0	0
Y (ppm)	19	22	45	39	32	40	36
ΣREE (ppm)	742	770	712	795	713	799	739

Note: bdl = below detection limit.

Table 2. LA ICP MS results of SMIs hosted in augite and glassy matrix of the Nyiragongo lava 2002. Concentrations represent average values of 2 - 7 single melt inclusions for four assemblages (N, H, P, A) and the standard deviation is approximately 10% of the average (e.g.: For N-assemblage, SiO₂ = (31.7 ± 3.2) wt%); Alk means alkali as the sum of Na₂O + K₂O; (n) = number of single SMI in a given assemblage.

LA ICPMS results of Nyiragongo 2002 for SMIs and lava glassy matrix								
Geodynamic context:	Rift							
Rift zone:	East African Rift System							
Rift zone target:	Western Branch (WB)							
Locality:	Goma (North Kivu)/DRC							
Volcano:	Nyiragongo							
Volcano type:	Stratovolcano							
Samples	DM 14UM-N -SMI (4)	DM 14UM-H -SMI (2)	DM 14UM-P -SMI (3)	DM 14UM-A -SMI (7)	DM 14UM-N -GLASS	DM 14UM-H -GLASS	DM 14UM-P -GLASS	DM 14UM-A -GLASS
Major elements								
SiO ₂ (wt%)	31.14	31.33	30.58	31.76	40.75	40.90	38.07	40.35
TiO ₂ (wt%)	1.38	1.67	1.38	0.20	1.78	0.92	1.68	2.66

Continued

Al ₂ O ₃ (wt%)	9.14	7.88	8.85	9.44	7.81	24.31	22.88	20.77
FeOt (wt%)	2.36	2.17	2.16	2.75	4.55	2.54	3.85	2.17
MnO (wt%)	0.10	0.10	0.10	0.20	0.49	0.20	0.39	0.20
MgO (wt%)	20.14	24.14	21.93	28.12	6.92	5.39	7.40	13.98
CaO (wt%)	33.20	30.25	32.65	24.48	32.64	11.70	12.52	10.73
Na ₂ O (wt%)	1.38	1.38	1.28	1.77	3.86	7.32	7.89	5.61
K ₂ O (wt%)	1.08	0.99	0.98	1.18	0.99	6.51	5.03	3.15
P ₂ O ₅ (wt%)	0.10	0.10	0.10	0.10	0.20	0.20	0.30	0.39
Total (wt%)	100.0	100.0	100.0	100.0	100.0	100.0	100.0	100.0
Na ₂ O + K ₂ O (wt%)	2.5	2.4	2.3	2.9	4.8	13.8	12.9	8.8
Na ₂ O/K ₂ O	1.3	1.4	1.3	1.5	3.9	1.1	1.6	1.8
Mg# [Mg/(Mg + Fe)]	0.9	0.9	0.9	0.9	0.6	0.7	0.7	0.9
Minor elements								
Sc (ppm)	241	231	213	14	9	4	16	48
V (ppm)	508	457	499	917	162	81	454	317
Cr (ppm)	2956	5987	1842	399	8	11	15	176
Be (ppm)	bdl	bdl	bdl	bdl	10	12	bdl	bdl
B (ppm)	63	77	49	62	50	56	54	41
Co (ppm)	66	70	66	291	86	40	67	68
Ni (ppm)	296	251	266	2636	57	84	101	133
Cu (ppm)	4	4	41	13	39	132	170	115
Zn (ppm)	45	39	46	213	455	468	391	204
Hf (ppm)	10	8	9	8	18	1	12	8
Ta (ppm)	0	0	0	0	30	19	21	3
Re (ppm)	1	1	1	1	1	1	2	bdl
Ir (ppm)	0	0	0	0	0	0	0	bdl
Ga (ppm)	21	16	20	2	39	42	45	39
Rb (ppm)	1	1	1	1	17	334	130	41
Sr (ppm)	241	220	241	658	11067	13321	5854	816
Y (ppm)	18	17	19	3	93	41	47	46
Zr (ppm)	168	135	175	219	1215	198	776	324
Nb (ppm)	1	1	1	3	420	461	240	52
Mo (ppm)	3	3	21	3	4	14	5	4
Sn (ppm)	8	6	bdl	bdl	6	8	8	4
Sb (ppm)	bdl	bdl	bdl	bdl	3	bdl	bdl	bdl
Cs (ppm)	1	5	18	1	1	4	9	1
Ba (ppm)	4	4	4	23	2761	9732	1330	617
W (ppm)	1	2	bdl	2	2	6	7	bdl
Pt (ppm)	2	2	2	3	2	3	3	bdl

Continued

Pb (ppm)	1	1	8	1	6	22	7	6
La (ppm)	10	8	10	2	394	306	199	42
Ce (ppm)	37	28	38	54	767	529	422	90
Pr (ppm)	6	6	6	1	81	49	45	11
Nd (ppm)	35	31	37	3	270	151	160	44
Sm (ppm)	9	9	9	10	40	22	25	11
Eu (ppm)	2	2	2	2	13	7	7	3
Gd (ppm)	7	7	7	7	27	11	17	9
Tb (ppm)	1	1	1	1	4	2	3	1
Dy (ppm)	5	4	5	5	22	10	11	9
Ho (ppm)	1	1	1	1	4	2	2	2
Er (ppm)	1	2	2	2	10	4	5	4
Tm (ppm)	0	0	0	1	2	1	1	1
Yb (ppm)	2	2	2	4	12	3	5	5
Lu (ppm)	0	0	0	1	2	0	1	1
S (ppm)	103	150	315	196	1851	1344	1538	2634
F (ppm)	350	452	339	365	1009	1256	1142	3315
Cl (ppm)	343	259	270	670	250	345	607	806
ΣREE (ppm)	117	101	119	93	1646	1096	902	231

Note: bdl = below detection limit.

Table 3. EPMA analytical results of mineral phases including Augite (core and rim), magnetite and glassy matrix of the Nyiragongo lava 2002 (Concentrations of major oxides are expressed in wt%).

Sample (Mineral)	SiO ₂	Al ₂ O ₃	FeO _t	MnO	Cr ₂ O ₃	MgO	K ₂ O	CaO	TiO ₂	Na ₂ O	P ₂ O ₅	Total	Mg#
DM14UM-1A1-Core (Augite)	49.52	4.96	4.61	0.04	0.41	14.96	0.01	23.59	1.65	0.24	0.00	100.00	0.76
DM14UM-1B1-Rim (Augite)	41.99	8.17	6.81	0.14	0.04	12.06	0.02	25.98	3.45	0.35	0.00	99.02	0.64
DM14UM-1A2-Core (Augite)	49.82	5.06	4.68	0.05	0.41	15.96	0.01	22.99	1.54	0.12	0.00	100.66	0.77
DM14UM-1B2-Rim (Augite)	40.99	7.06	7.06	0.12	0.06	12.86	0.00	28.00	3.09	0.25	0.00	99.52	0.65
DM14UM-1A3-Core (Augite)	48.72	4.22	4.03	0.09	0.48	14.76	0.01	24.69	1.25	0.30	0.00	98.58	0.79
DM14UM-1B3-Rim (Augite)	41.59	7.87	6.99	0.24	0.09	13.86	0.03	25.18	4.04	0.27	0.00	100.19	0.66
DM14UM-1A4-Core (Augite)	48.92	4.17	5.13	0.07	0.44	15.26	0.02	23.00	1.00	0.20	0.00	98.25	0.75
DM14UM-1B4-Rim (Augite)	42.09	8.37	7.16	0.19	0.05	12.56	0.00	25.98	2.99	0.25	0.00	99.66	0.64
DM14UM-1A5-Core (Augite)	47.32	5.07	4.51	0.03	0.51	14.77	0.01	24.05	2.65	0.19	0.00	99.15	0.77
DM14UM-1B5-Rim (Augite)	40.69	8.00	6.11	0.16	0.08	13.16	0.00	27.08	4.33	0.31	0.00	99.93	0.68
DM14UM-1A6-Core (Augite)	50.12	4.66	5.21	0.10	0.50	16.16	0.04	21.89	0.85	0.21	0.00	99.76	0.76
DM14UM-1B6-Rim (Augite)	40.81	8.05	7.21	0.20	0.10	12.16	0.01	28.16	3.01	0.34	0.00	100.07	0.63
DM14UM-1A7-Core (Augite)	47.66	6.48	5.56	0.03	0.16	14.23	0.00	23.57	1.99	0.27	0.00	99.98	0.72
DM14UM-(Glassy matrix)	41.70	33.65	0.81	0.00	0.04	0.14	7.35	0.44	0.02	15.85	0.00	100.00	0.15
DM14UM-Magnetite	0.00	6.96	67.85	0.82	0.06	5.72	0.00	0.00	18.56	0.01	0.00	100.00	0.08

4. Results

4.1. Rock Petrography, Mineralogy, and Field Relationships

The Nyiragongo volcano owing a long history of volcanic activities, have emitted huge volumes of lavas through the central crater and shutter cones as well (**Figure 4(c)**, **Figure 4(d)**). This conic volcanic edifice with a circular central crater is a stratovolcano that consisted of overridden quenched lavas spilled out during all the past times of volcanic activities (**Figure 4(a)**, **Figure 4(b)**). The Nyiragongo 1977 and 2002 lavas, macroscopically appear as dark rough mass of vitric aspects, hosting abundant degassing pores, and where crystallized phenocrysts

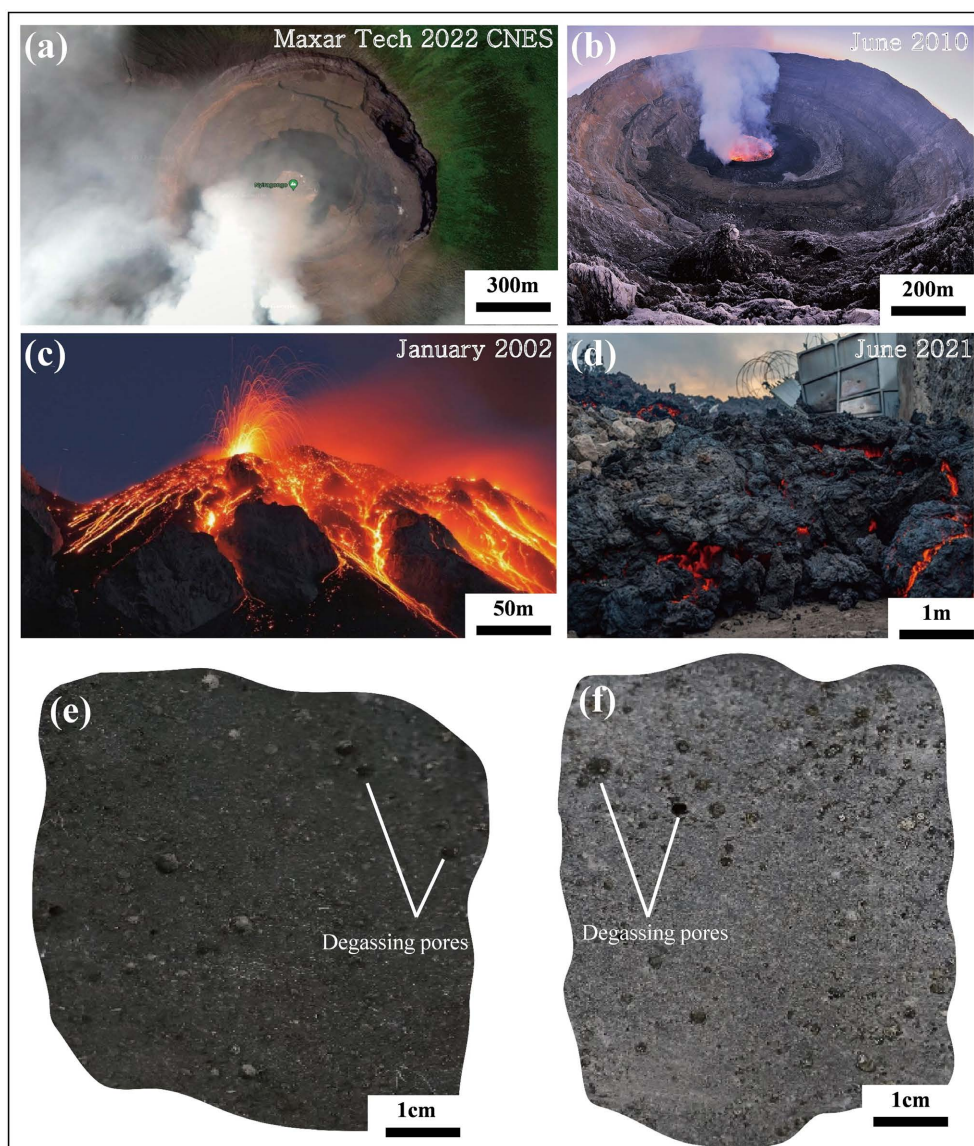


Figure 4. Photo macrographs of the Nyiragongo volcano and lava samples: (a-b) Satellite views of the magma crater lake and permanent out degassing fumes; (c) A photo of Nyiragongo volcanic eruption 2002; (d) A photo of flowing liquid products of the recently erupted Nyiragongo 2021 in the Goma surrounding city showing the continuum of rapid cooling of the magma; (e-f) Nyiragongo lava samples of respectively 1977 and 2002 volcanic eruptions showing degassing pores.

are barely distinguishable (**Figure 4(e)**, **Figure 4(f)**). The petrographic compositions of the out spilled volcanic materials have not significantly changed during the last decades of its magmatic activities. As the precedent lavas, the 1977 and 2002 emitted lavas showed weakly porphyritic textures that consist of phenocrysts (5% - 10%), microlites (20% - 30%), degassing pores (5% - 10%) and glassy matrix (50% - 60%). Phenocrysts sizing up to 0.5 - 1 cm, consist of essentially clinopyroxene (augite) and rarely olivine (Fo.70 - 85). Microlites are constituted of clinopyroxene (augite), disseminated magnetite, olivine, melilite, phlogopite and plagioclase in a roughly in decreasing order of their relative abundance (**Figures 5(a)-(f)**). The 1977 lava showed additionally sporadic aggregates of feldspathoids (nepheline, rarely leucite) and rare plagioclase microlites. Glassy matrix occurring as dominantly groundmass is widely tapped by crystalline phenocrysts, microlites and degassing pores (**Figures 5(a)-(d)**).

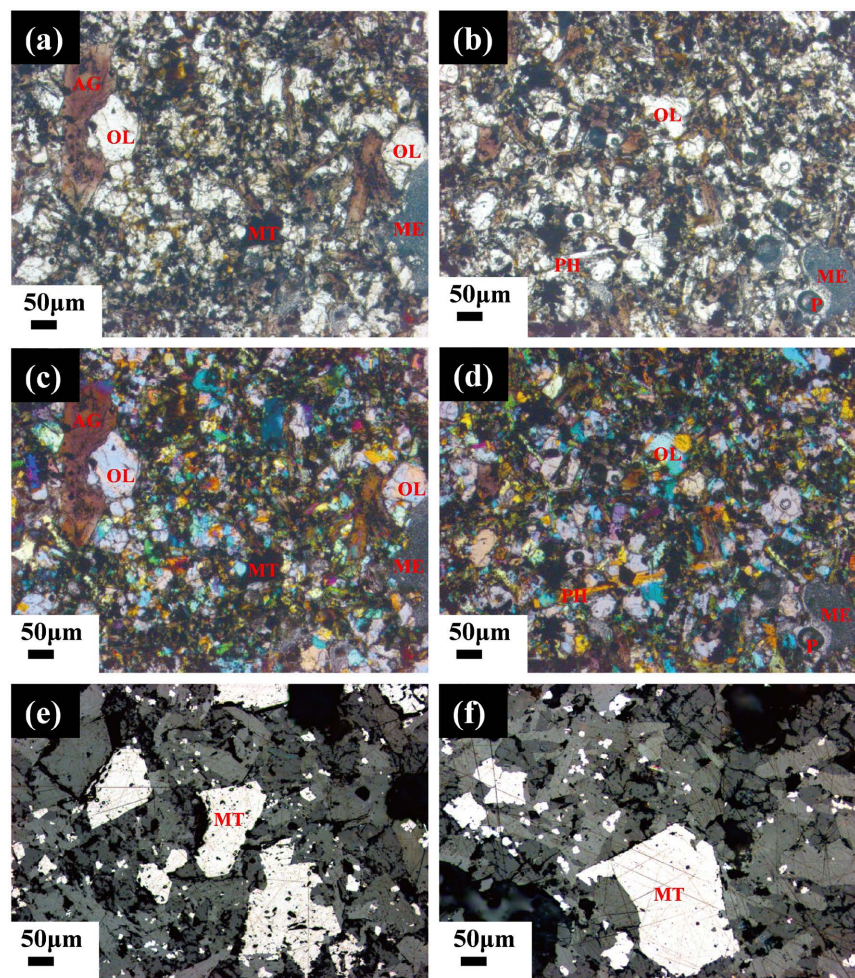


Figure 5. Photomicrographs of the Nyiragongo lava 2002: (a-b) A transmitted plane polarized light (PPL) images and (c-d) A transmitted cross polarized light (XPL) images showing the presence olivine, augite, phlogopite, melilite, microlite, degassing pores, opaques and glassy matrix; (e-f) A reflected cross polarized light (XPL) images showing disseminated magnetite. (OL = olivine, AG = augite, ME = melilite, PH = phlogopite, MT = magnetite, P = degassing pore).

The 1977 and 2002 show relatively similar mineralogical compositions; however, the slight difference resides in feldspathoid type and abundances where nepheline and leucite dominantly occurred in 1977 lava whereas melilite dominated in 2002 lava. Towards their mineralogical assemblages, the Nyiragongo 1977 and 2002 lavas are globally foidic rocks especially nephelinites or melilite nephelinites.

4.2. Silicate Melt Inclusion Petrography

The silicate melt inclusion study was carried out essentially in the Nyiragongo 2002 lava that hosted well-crystallized phenocrysts of clinopyroxene (augite) sizing up to 1cm of diameter were observable. These phenocrysts consisted of mainly euhedral augite and rarely olivine; and the bigger the phenocryst the greater the chance to find good and useful melt inclusions. Despite their sizes, few phenocrysts of augite showed SMIs occurrences and they were targeted for subsequent microanalyses. Microscopic observations of doubly-side polished sections of augite showed the presence of fully and partially trapped melt inclusions. Partially quenched inclusions were dominant (**Figures 6(a)-(d) & Figure 6(f)**) while fully quenched melt inclusions were rarely observed (**Figure 6(e)**). Augite hosting SMIs showed diverse sizes, features, and shapes. SMIs of more than 25 μm were selected LA-ICP-MS analyses (**Figure 6(d) & Figure 6(f)**). SMIs were spatially trapped as single inclusion body (**Figure 6(e), Figure 7(b)**), an assemblage of aligned inclusion bodies (**Figure 6(c), Figure 6(d)**), a cluster or scattered inclusions (**Figure 6(a), Figure 6(b) & Figure 6(f), Figure 7(c)**). A Raman laser and EPMA analyses have identified the host mineral to be a clinopyroxene as of augite (**Figure 8(a)**). A Raman spectroscopy on silicate melt inclusions showed the presence of gas species and sulfide metals such as carbon dioxide (CO_2), methane (CH_4), water (H_2O), sulfur dioxide (SO_2), anhydrate (CaSO_4), and chalcopyrite (CuFeS_2), (**Figure 8(b)**). The quasi-scarcity of phenocrysts combined with the infrequency of big silicate melt inclusions lead to the non-abundance petrographic and chemical data for these studied lavas.

4.3. Rock, Glassy Matrix, and SMI Chemistry

The Nyiragongo lavas of 1977 and 2002, showed globally a chemical proximity of major elements as of being poor in SiO_2 (38.4 - 39.5 wt%), MgO (3.0 - 4.1 wt%), and relatively rich in Fe_2O_3 (13.8 - 14.1 wt%), CaO (11.0 - 12.3 wt%), sum of alkalis $\text{Na}_2\text{O} + \text{K}_2\text{O}$ (10.3 - 11.9 wt%) and moderated amounts of P_2O_5 (1.5 - 1.7 wt%) and TiO_2 (1.6 - 2.1 wt%), (**Table 1**). In the total alkalis versus silica diagram, the Nyiragongo 1977 and 2002 are closely plotted in the field of foidites especially melilite nephelinites (**Figure 9**). The 100 Mg#, $[\text{Mg}/(\text{Mg} + \text{Fe total}) \times 100]$ is neatly below 30 (18 - 23), $\text{Na}_2\text{O}/\text{K}_2\text{O}$ (0.9 - 1.2) and LOI (H_2O) being low (1.0 - 1.6 wt%), (**Table 1**). The chemical composition of traces of Nyiragongo 1977 and 2002 lavas is clearly indistinguishable as well. They both show relatively poor concentrations of Ni (40 - 50 ppm), Cr (15 - 21 ppm), and Co (22 - 45

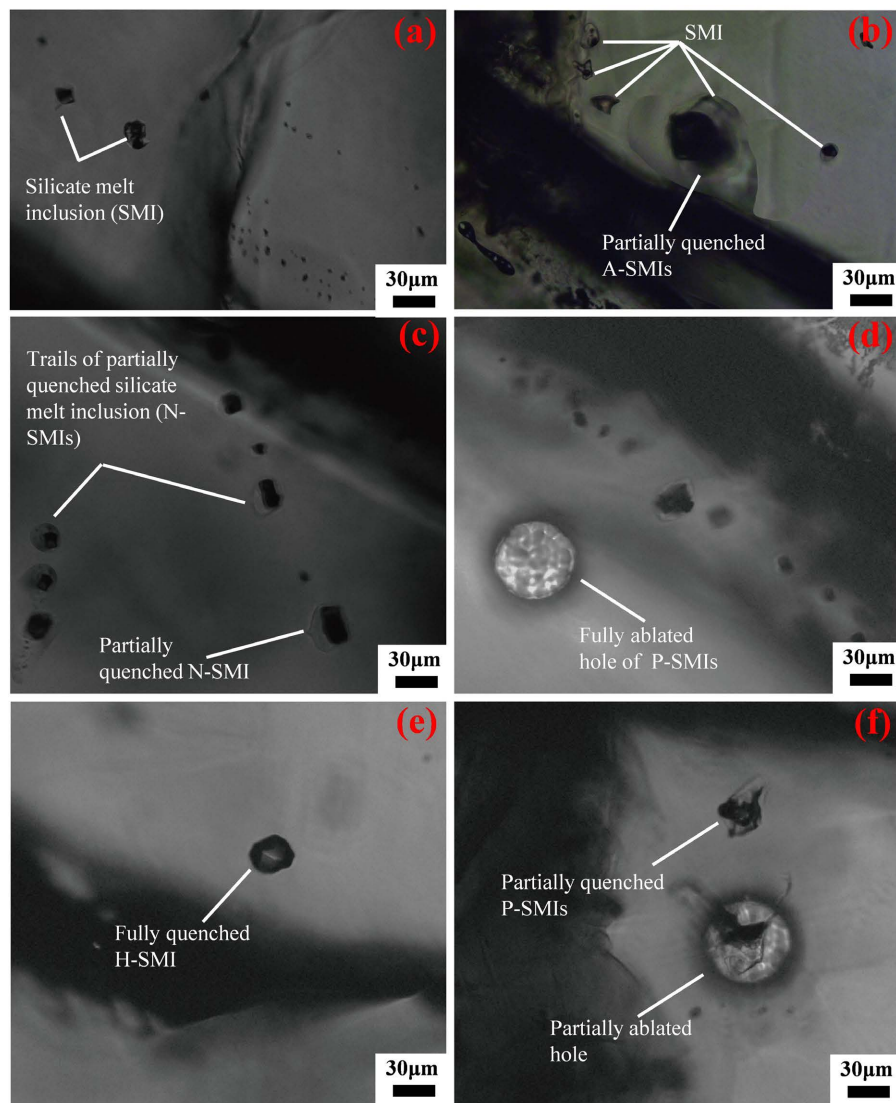


Figure 6. Microphotographs of silicate melt inclusions hosted in augite from Nyiragongo lava 2002: (a-b) A cluster of partially quenched silicate melt inclusions for the A-assembly displaying small and big sizes; (c-d) Trails of partially silicate melt inclusions for N-assembly and the hole of totally laser ablated melt inclusion for M-assembly; (e) A fully quenched melt inclusion-H, spatially trapped as a singly body ; (f) A cluster of partially quenched melt inclusions for P-assembly displaying a partially ablated hole.

ppm); however, moderated concentrations in V (303 - 450 ppm), Cu (169 - 211 ppm), Zr (299 - 401 ppm) and Zn (122 - 245 ppm), (**Table 1**). Low ratios of Rb/Sr (0.04 - 0.06) and Zr/Nb (1.53 - 2.12) while Sr/Rb (17.13 - 28.09) and Ba/Rb (16.38 - 20.60) are relatively high. The REE concentrations of the Nyiragongo 1977 and 2002 are moderately high as of the sum (Σ REEs) is 712 - 799 ppm. Chondrite normalized ratios of $(\text{Tb/Yb})_N$ is 1.6 - 2.7, $(\text{Gd/Lu})_N$ is 3.2 - 4.3, $(\text{Sm/Yb})_N$ is 4.8 - 8.9, $(\text{Ce/Yb})_N$ is 31.5 - 43.8, and $(\text{La/Yb})_N$ is 42.6 - 51.4. In addition to the mineralogical affinity, the overall chemical affinities of the Nyiragongo 1977 and 2002 lavas are their alkalinity (sodi-potassic) and undersaturation in silica as mafic/ultramafic alkaline rocks.

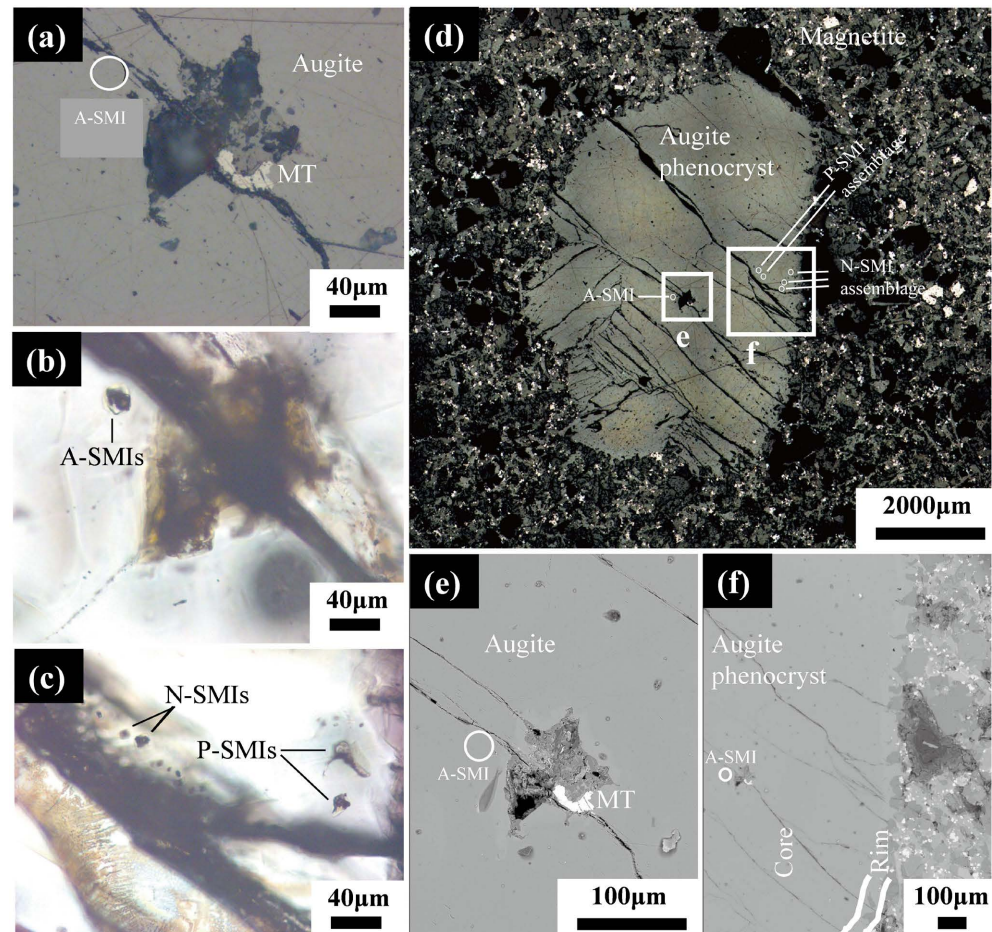


Figure 7. Photomicrographs of silicate melt inclusions and hosting mineral phenocrysts in the Nyiragongo 2002 lava: (a) A reflected plane polarized light (PPL) microphotograph showing a selected location of SMI-A assemblage and inclusion of magnetite hosted in augite phenocryst; (b) A transmitted cross polarized light (XPL) microphotograph showing a partially quenched SMI-A assemblage and an opaque magnetite hosted in augite; (c) A transmitted PPL microphotograph displaying an assemblage of silicate melt inclusions hosted in augite; (d) A reflected XPL microphotograph showing glassy matrix, microlite, disseminated magnetite, and augite phenocryst with mapped silicate melt inclusion locations; (e) Backscattered electron (BSE) image of a selected location of SMI-A assemblage and inclusion of magnetite hosted in augite phenocryst; (f) BSE image of the lava showing a rimmed augite phenocryst hosting SMI, disseminated magnetite, glassy matrix and other microlites. The augite rim is iron and calcium-rich zone of the crystal. (A, N and P letters are used for silicate melt inclusion assemblages; SMI = silicate melt inclusion, MT = magnetite).

The Nyiragongo 2002 glassy matrix, showed commonly chemical proximities of majors with whole-rock; however, they displayed slight enrichment in SiO_2 (38.6 - 41.2 wt%), CaO (10.9 - 33.0 wt%), poor MgO (5.3 - 14.2 wt%), and relatively poor in Fe_2O_3 (2.2 - 4.6 wt%), sum of alkalis $\text{Na}_2\text{O} + \text{K}_2\text{O}$ (4.9 - 13.6 wt%), P_2O_5 (0.2 - 0.4 wt%) and TiO_2 (0.9 - 2.7 wt%), (**Table 2**). In the total alkalis versus silica diagram, the Nyiragongo 2002 glassy matrix is closely plotted in the fields of tephro-basalts and foidites especially nephelinites (**Figure 9**). The 100 Mg#, $[\text{Mg}/(\text{Mg} + \text{Fe total}) \times 100]$ lies between 60 - 86, $\text{Na}_2\text{O}/\text{K}_2\text{O}$ (1.6 - 3.9), (**Table 2**). The chemical composition of minor elements of Nyiragongo 2002 glassy

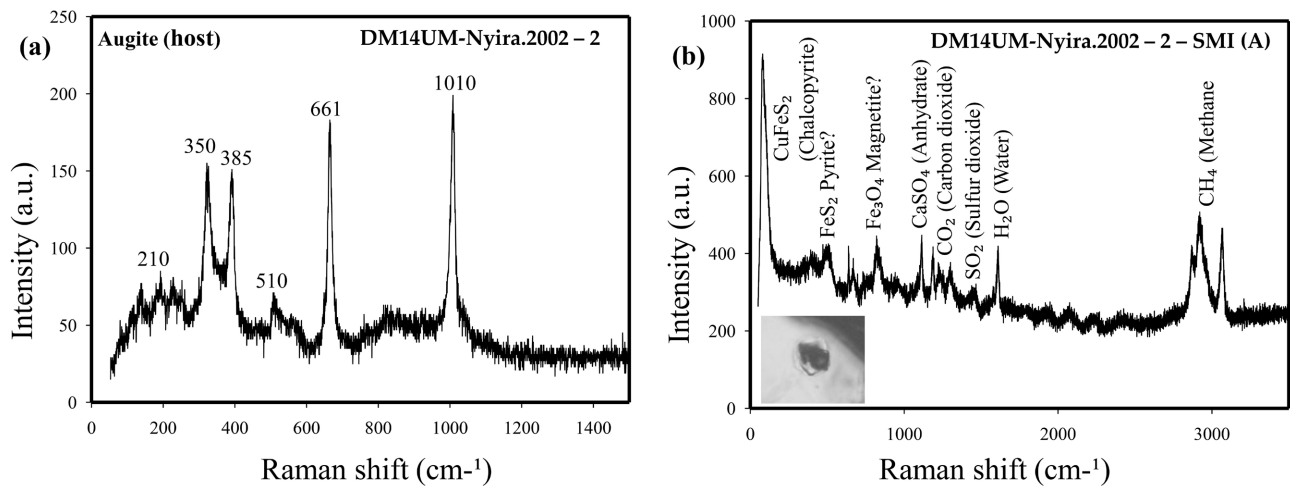


Figure 8. (a) A Raman laser on lava phenocrysts showing consistent peak signals of augite; (b) A Raman laser on silicate melt inclusion showing the presence carbon dioxide (CO₂), methane (CH₄), water (H₂O), sulfur dioxide (SO₂), anhydrate (CaSO₄), and sulfide minerals such as chalcopyrite (CuFeS₂).

matrix is not far different of the bulk rock lava 2002. The glassy matrix showed relatively low to moderate concentrations in S (1851 - 2634 ppm) and halogens such as Cl (250 - 805 ppm) and F (1009 - 3315 ppm). Minor elements including Ni (57 - 133 ppm), Cr (8 - 176 ppm), and Co (40 - 86 ppm) have slightly increased in concentrations. Moreover, concentrations in V (81 - 317 ppm), Cu (39 - 170 ppm), have slightly decreased while Zr (198 - 1215 ppm) and Zn (204 - 454 ppm) showed higher concentrations compared to the whole-rock, (**Table 2**).

Same as in the whole-rock, ratios of Rb/Sr (0.002 - 0.050) and Zr/Nb (0.43 - 6.21) are low while Sr/Rb (17.87 - 658.00) and Ba/Rb (10.27 - 29.12) are relatively high. The REE concentrations of the Nyiragongo 2002 glassy matrix are low to moderately high as of the sum (Σ REEs) is 231 - 1646 ppm. Chondrite normalized ratios of (Tb/Yb)_N is 1.2-2.3, (Gd/Lu)_N is 1.9 - 3.4, (Sm/Yb)_N is 2.5 - 7.2, (Ce/Yb)_N is 5.1 - 42.7, and (La/Yb)_N is 6.3 - 64.3. The glassy matrix chemistry is globally similar with whole-rock especially for major elements; minor differences are found in trace element compositions.

The Nyiragongo 2002 silicate melt inclusions (SMIs), showed unambiguously distinctive chemical compositions of major and minor elements compared to the whole-rock lavas and glassy matrix.

SMI showed neatly poor concentrations in SiO₂ (31.1 - 32.3 wt%), P₂O₅ (0.0 - 0.1 wt%), Fe₂O₃t (2.2 - 2.8 wt%), Al₂O₃ (8.0 - 9.6 wt%), and the sum of alkalis Na₂O + K₂O (2.3 - 3.1 wt%); whereas they show a relative enrichment CaO (24.9 - 33.8 wt%), MgO (20.3 - 28.6 wt%), and variable TiO₂ (0.2 - 1.7 wt%) compared to the whole-rock and glassy matrix (**Table 2**). In the total alkalis versus silica diagram, the Nyiragongo 2002 SMIs are closely plotted in the field of picro-basalts or picrites (**Figure 9**). The 100 Mg#, [Mg/(Mg + Fe total) × 100] lies between 90 - 92, Na₂O/K₂O (1.3 - 1.5), (**Table 2**).

The SMIs showed relatively low concentrations of S (103 - 196 ppm) and halogens such as Cl (259 - 700 ppm) and F (339 - 452 ppm) compared to the whole-rock

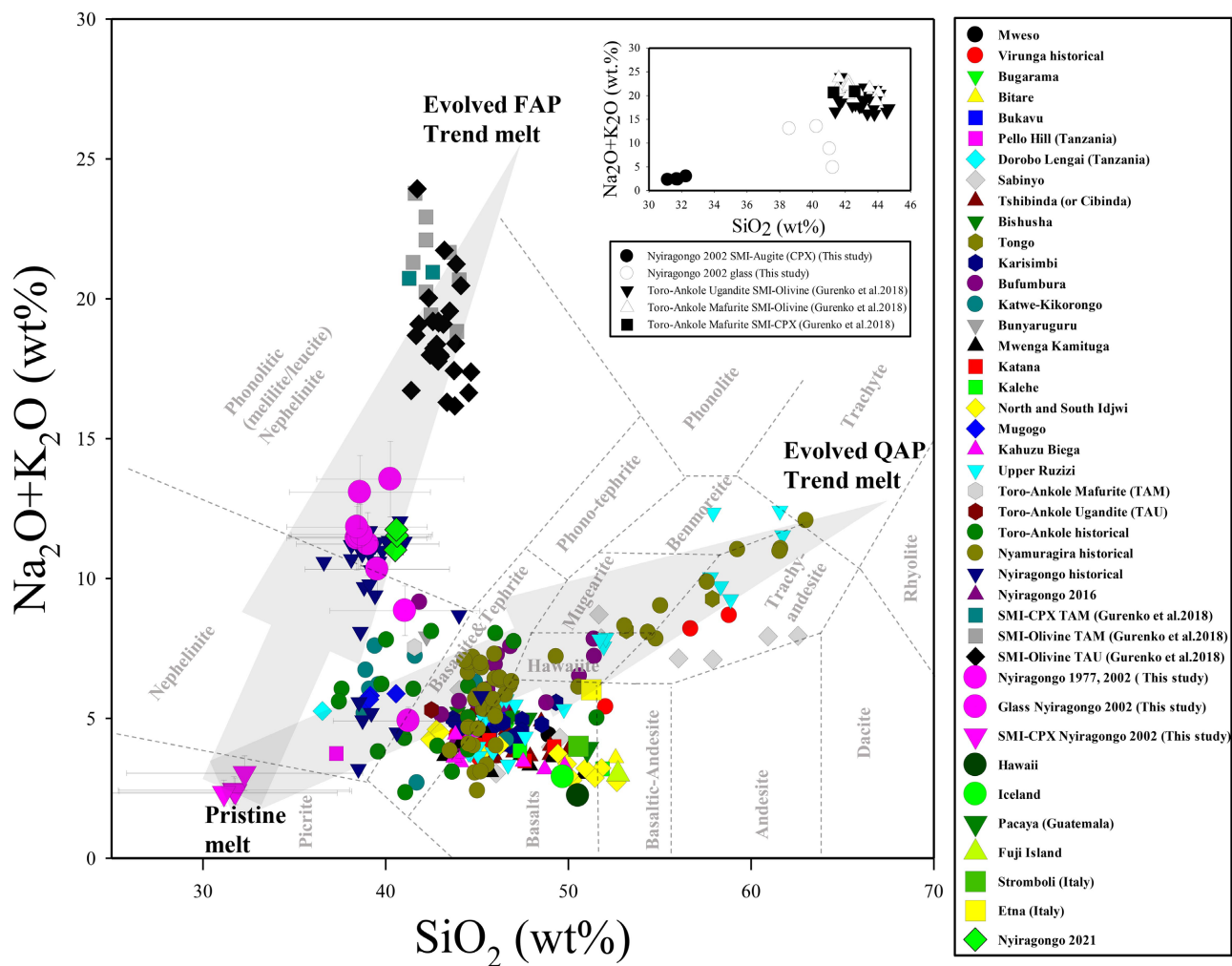


Figure 9. Total alkalis versus silica diagram showing silicate melt inclusions and whole rock major element analyses of compiled Nyiragongo 1977 and 2002 lavas and other volcanic rocks from the East African Rift System in the western branch. The Nyiragongo picritic melts (red diamond symbols), are interpreted as more likely pristine melt having <40 wt% SiO₂, >18 wt% MgO, are compositionally poor in total alkalis Na₂O + K₂O up to 3 wt% compared to the evolved Toro-Ankole nephelinitic melts where the total alkali is more than 15 wt%. (SMI = silicate melt inclusion, CPX = clinopyroxene, Oliv. = olivine FAP = Feldspathoid-K-feldspar-Plagioclase, QAP = Quartz-K-feldspar-Plagioclase). Gray arrows show the evolution or differentiation of the magma from pristine to evolved melts. Data of Nyiragongo 1977 and 2002 lavas and SMIs (this study) and 2021 lava are expressed as average ± standard deviation.

and glassy matrix. Minor elements such as Ni (251 - 2636 ppm), Cr (399 - 2956 ppm), V (457 - 917 ppm) and Co (66 - 291 ppm) showed higher concentrations compared to the 2002 whole-rock lava and glass. However, Cu (4 - 41 ppm), Zr (135 - 219 ppm) and Zn (39 - 212 ppm) displayed lower concentrations compared to both whole-rock and glassy matrix, (Table 2). Additionally, ratios such as Rb/Sr (0.002 - 0.004) and Ba/Rb (4.10 - 16.45) are relatively lower while Zr/Nb (68.08 - 139.34) and Sr/Rb (253.51 - 473.43) are relatively higher compared to the whole-rock and glassy matrix values. The REE concentrations of the Nyiragongo 2002 SMIs are relatively low as of the sums (Σ REEs) are 43 - 119 ppm. SMI chondrite normalized ratios such as (Tb/Yb)_N being 1.5 - 2.1, (Gd/Lu)_N

ranging 1.5 - 2.8, and $(\text{Sm}/\text{Yb})_N$ being 3.1 - 4.7, are slightly similar with the whole-rock and glassy matrix values; while $(\text{Ce}/\text{Yb})_N$ being 0.3 - 4.9, and $(\text{La}/\text{Yb})_N$ 0.5 - 3.6 are far lower and different compared to the whole-rock and glass.

In summary, the petrographic and chemical compositions of the Nyiragongo (1977 and 2002) whole-rock, glassy matrix consisted of alkaline-rich nephelinites whereas SMIs are different and showed a picritic signature.

4.4. Mineral Features and Chemistry

The Nyiragongo 1977 and 2002 lavas showed essentially phenocrysts of clinopyroxene notably augite. The identification of augite was performed under Raman laser and microscopic observations (**Figures 7(a)-(d)** and **Figure 8(a)**). The BSE image of the studied augite showed distinctive parts of the mineral colored in grey dark for the core and grey light for the rim (**Figure 7(e)**, **Figure 7(f)**). This difference inside the mineral feature was slightly reflected in the chemistry as well. The EPMA analyses (**Table 3**) showed that the rimmed part was relatively poor in SiO_2 (40.7 - 42.1 wt%) Cr_2O_3 (0.4 - 0.5 wt%) and MgO (12.1 - 13.9 wt%) compared to the core as of SiO_2 (47.3 - 50.1 wt%), Cr_2O_3 (0.0 - 0.1 wt%) and MgO (14.8 - 16.2 wt%). The 100 Ca#, $[\text{CaO}/(\text{CaO} + \text{MgO}) \times 100]$ of the core and the rim are respectively 58 - 63 and 65 - 70; and the 100 Mg#, $[\text{Mg}/(\text{Mg} + \text{Fe total}) \times 100]$ values of core and rim parts are 75 - 79 and 63 - 68 respectively. However, the rimmed part was relatively enriched in CaO (25.2 - 28.2 wt%), TiO_2 (3.0 - 4.0 wt%) and MnO (0.1 - 0.2 wt%) compared to the core as of CaO (21.9 - 24.7 wt%), TiO_2 (0.9 - 2.7 wt%) and MnO (0.0 - 0.1 wt%). Augite hosted inclusions of mineral such as magnetite (**Figure 7(a)** & **Figure 7(e)**). The chemical composition of magnetite consisted of mainly iron and where average concentrations are Fe_2O_3 (67.9 wt%), TiO_2 (18.6 wt%), Al_2O_3 (7.0 wt%), MgO (5.7 wt%), and MnO (0.8 wt%), (**Table 3**). This titanomagnetite was the abundant opaque minerals of the Nyiragongo 1977 and 2002 lavas.

4.5. REE Patterns of Whole Rock, Glass, and SMIs

REE patterns of the Nyiragongo 1977 and 2002 whole-rock and glass showed globally a regular feature with a decline starting from light-REE to heavy-REE. However, SMI feature trend of REE showed a relative enrichment of medium-REE compared to light-REE; and compared to the whole-rock and glassy matrix, SMIs displayed lower concentrations and were plotted in lower levels. REE multi-element diagrams as a broad feature combine rare earth elements with other major or trace elements. Instead of using numeral elements, have selected a total of 9 that include rare earth elements (REE), large ion lithophile elements (LILE) and high field strength elements (HFSE) as of Th, Ce, Zr, Rb, La, Eu, Sm, Sr and Nb and reordered in a serial sequence called a contracted-spider diagram. The plotted results displayed globally a W-feature that characterized volcanic rocks of the western branch of the EARS (**Figures 10(a)-(d)**). This REE W-feature appeared in few samples of the southern part of the eastern branch such as historical data from Tanzania volcanoes (Pello hill and Dorobo Lengai), (**Figure 10(a)**).

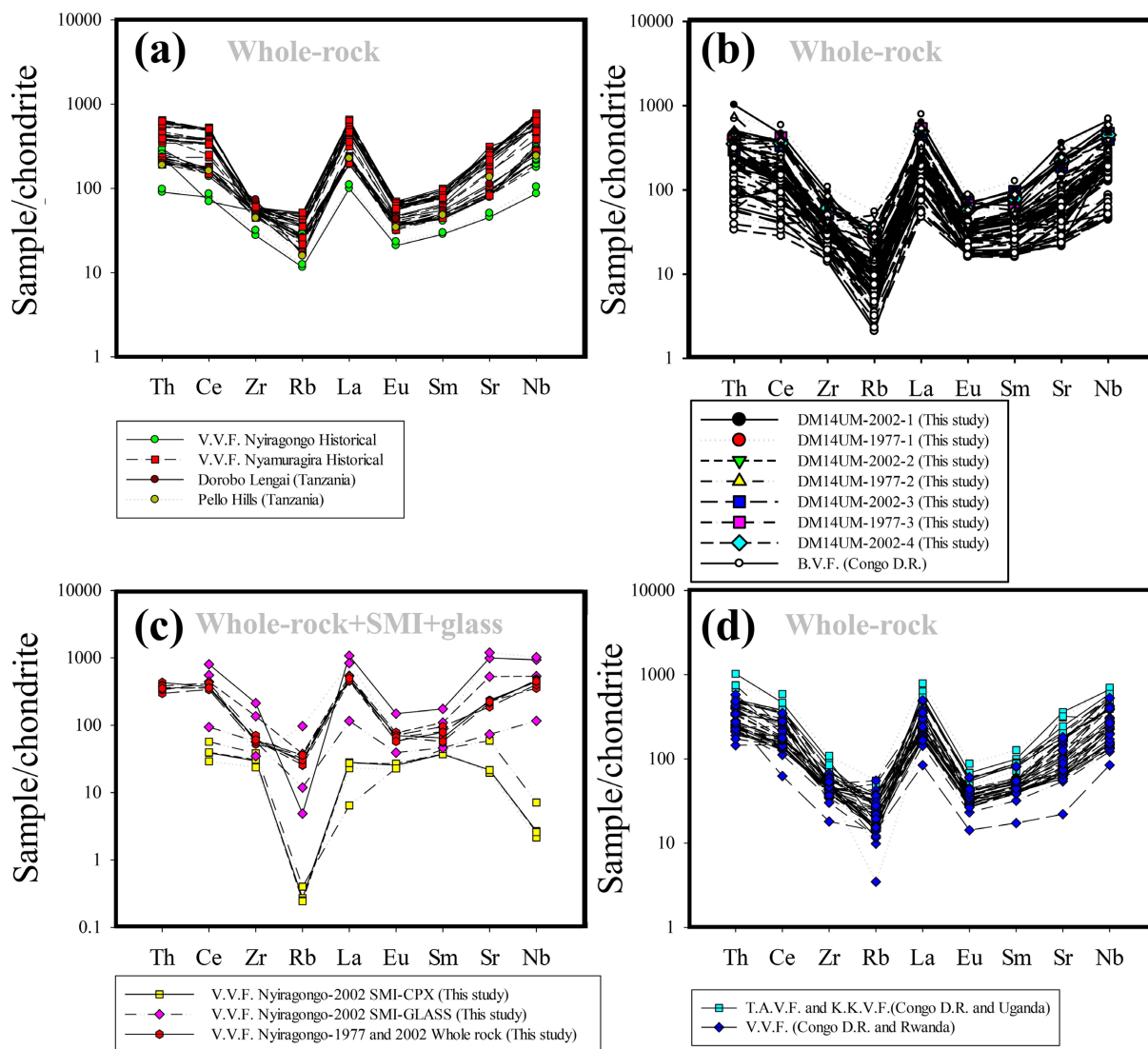


Figure 10. Contracted multi-element REE patterns of compiled EARS lavas showing a characteristically W-feature: (a) Virunga volcanic field in the western branch and Tanzanian Dorobo Lengai and Pello Hill in the eastern branch; (b) Nyiragongo 1977 and 2002 lavas in the Virunga volcanic field, and lavas from the Bukavu volcanic field, (c) Nyiragongo 2002 SMI, Glass and whole rock, (d) Toro-Ankole volcanic field and Virunga volcanic field lavas. (*SMI* = *silicate melt inclusion*, *CPX* = *clinopyroxene*, *V.V.F.* = *Virunga volcanic field*, *B.V.F.* = *Bukavu volcanic field*, *T.A.V.F.* = *Toro-Ankole volcanic field*, *K.K.V.F.* = *Katwe-Kikorongo volcanic field*). SMIs show relatively non-identical patterns of contracted spider diagram compared to whole rock lavas.

The contracted-spider diagram showed of whole-rock and glassy matrix showed a fractionation of elements with a relative enrichment of Th, La, and Nb while Rb and Eu were depleted (**Figures 10(a)-(d)**). However, the SMI contracted-spider diagram displayed an irregular different feature in which the melt was slightly fractionated and showed a depletion of Rb and Nb (**Figure 10(c)**).

4.6. SMIs as Volcanic System Geothermometer, and Lava Age Records

Geothermometers of volcanic systems employ various methods and approaches

such as mineral-mineral pairs, mineral-liquid pairs or trace element distributions between the melt-mineral to estimate temperatures of the risen melts [47] [48] [49] [50] [51]. In this study, we have used the chemistry especially the MgO concentrations of the trapped melt inclusions and glassy matrix to estimate the melt temperature. The empirical formula $[T(^{\circ}\text{C}) = 20.1\text{MgO}_{\text{liq}} + 1014^{\circ}\text{C}]$ was used for the calculation of temperatures [47]. Estimated temperatures ranged $1355^{\circ}\text{C} - 1740^{\circ}\text{C}$ for SMIs and $1050^{\circ}\text{C} - 1333^{\circ}\text{C}$ for the glassy matrix (Figure 11(b)). A temperature difference of $305^{\circ}\text{C} - 407^{\circ}\text{C}$ was estimated between the deeper trapped SMIs and shallower evolved remaining melt (quenched as glassy matrix) after fractional crystallization. A comparison of various geothermometer results for the western branch of EARS is provided in this study (Figure 11(b)).

The Nyiragongo volcano yields hundreds of volcanic eruptions starting from the Cenozoic until the last June 2021. This volcano has a frequency of eruption

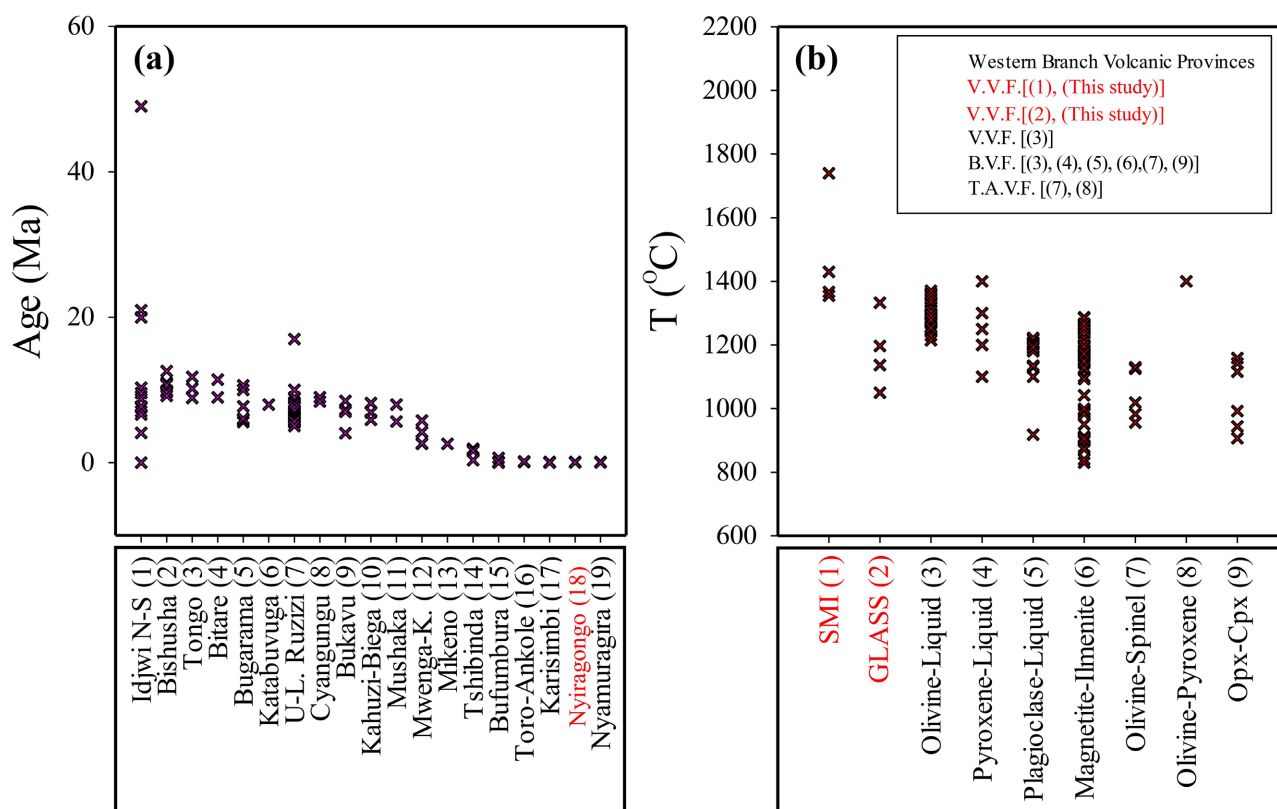


Figure 11. (a) A summarized ages of EARS western branch volcanic rocks of various sites, which rifting started from Cenozoic to Quaternary recent in the Congo D.R. and some neighboring eastern countries; ((1) = Tholeiite-Basalt-Nephelinite, (2) = Tholeiite-Basalt-Basanite-Hawaiiite-Mugearite, (3) = Basanite-Benmoreite, (4-6) = Tholeiite, (5) = Tholeiite-Basanite-Hawaiiite, (7) = Hawaiiite-Benmoreite-Phonolite-Trachyte-Tholeiite-Basalt-Basanite-Ankaratrite, (8) = Tholeiite (9) = Basalt-Basanite, (10) = Tholeiite-Basanite, (11) = Basanite-Hawaiiite, (12) = Tholeiite-Basalt-Basanite-Ankaratrite, (13) = Trachyte, (14) = Basalt-Basanite, (15) = Basalt-Basanite-Hawaiiite-Mugearite, (16) = Basalt-Basanite-Nephelinite, (17) = Basanite-Hawaiiite-Mugearite-Trachyte, (18) = Basanite-Melilite/Leucite Nephelinite (This study), (19) = Basanite-Hawaiiite-Benmoreite-Mugearite-Trachyte); (b) A comparison of temperature ranges between silicate melt inclusion, evolved glass and mineral pair methods. (1-2) are calculated using the simplified equation models $(T(^{\circ}\text{C}) = 20.1\text{MgO}(\text{liquid}) + 1014^{\circ}\text{C})$ [47] for volcanic system thermometers, (3) to (9) data are from [1]. (SMI = silicate melt inclusion, Cpx = clinopyroxene, Opx = orthopyroxene, V.V.F. = Virunga volcanic field, B.V.F. = Bukavu volcanic field, T.A.V.F. = Toro-Ankole volcanic field).

of approximately five years. Various methods of dating volcanic rock systems such as K-Ar, Ar-Ar on micas (phlogopite) have been used [6] [23]. This study concerned lavas of the volcanic eruptions 1977 and 2002 of the Nyiragongo volcano in the western branch (WB) of the EARS (**Figure 11(a)**).

5. Discussions

5.1. Pristine Melt Evidence, and Petro-Chemical Evolutions in the WB of EARS

The Nyiragongo 1977 and 2002 volcanic eruptions showed many similarities with the Kilauea volcano 2018 in terms of precursory signs of volcanic activities, the type and rheology of spilled magmatic products, and volcanic manifestations [52] [53] [54] [55] [56]. However, the petrographic and the geochemical characteristics are different as of high potassic melilite nephelinites for the Nyiragongo 1977 and 2002 whereas low potassic olivine picro-basalts for the Kilauea. The relationship between the rheology and phase equilibria of a picritic basalt from Kilauea volcano 2018 has been investigated at 1 atm along the QFM buffer, temperatures between 1270°C and 1180°C, olivine and minor spinel were the only liquidus phases, and the melt volume decreased from 85 to 74 vol%. At the olivine-spinel-plagioclase-clinopyroxene cotectic, the melt was consumed more rapidly dropping to 47 vol% at 1139°C [42] [54]. The rheology of the magma was non-Newtonian, and characterized by time-dependent, pseudoplastic behavior, and was consistent with power law flow or Bingham pseudoplastic behavior [42]. Non-Newtonian effects were most apparent when the crystal volume was greater than 25% and the shear rate was increasing; however, once stirred, the magma approached the Newtonian rheology with decreasing shear rate [42] [57].

The crystal volume of the Nyiragongo 1977 and 2002 lavas is small (approximately 10% - 20%), and the observed phenocrysts might have started forming far long-time and at deeper zones as well as at shallow depths, during and after the ascension; and gained bigger sizes compared to microlites that formed during rapid quenching of the magma at the surface. Phenocrysts hosting silicate melt inclusions offer good indications to retrace the chemical composition of the more likely initial melt and evolved magma products [33] [58] [59] [60] [61].

In the Nyiragongo lava 2002, trapped SMIs revealed a melt chemistry that suggest a primary melt composition [62] which is petrographically a picrite and host relatively low TiO₂-suite, K₂O, LILE concentrations such as Ba, Sr, and HFSE such as Zr (**Table 2**). However, picrites showing high Ti-suite (TiO₂ > 4%), moderate to high potassic (K₂O > 4%), and enriched in LILE and HFSE such as Ba (>1000 ppm), Sr (>2000 ppm) and Zr (>500 ppm), are perceived being not primary but evolved melts [63] [64] [65]. The rise of magma melts from the initially produced zone to the surface lead to various petrologic processes such as fractional crystallization, mineral sedimentations, crustal contamination, and metasomatism; and therefore, contributed to the production of various vol-

canic rocks found in rifting area [4] [23] [35] [59] [66]. In the western branch of the EARS, picritic rocks were rarely found; however, evolved terms such as tholeiites, nephelinites, tephro-basalts, hawaiites, mugearites, benmoreites, trachytes and phonolites were frequently and abundantly observed (**Figure 9**), [1]-[6] [11] [18] [20] [23] [32] [33] [36].

This suggest that a possibility to find picritic rocks is in the deep dyke systems which is closed to the R1 reservoir where the present silicate melt inclusions might have been trapped [7].

The whole-rock concentrations of F, Cl and S from samples of freshly erupted 2020 and 2021, free of hydrothermal phases, abundance of glassy materials, and Sr-Nd-Pb isotope data of Nyamuragira and Nyiragongo samples, are comprising highly primitive samples from both volcanoes [11] [18]. SMIs showed relatively low concentrations of S (103 - 196 ppm) and halogens such as Cl (259 - 700 ppm) and F (339 - 452 ppm) compared to the whole-rock and glassy matrix; and theses sulfur and halogen amounts are more likely correlated with mantle array ranges.

5.2. Ongoing Rifting, Magma Genesis, Fractional Crystallization, Magmatic Differentiation, and Modelling

The evolution of the rifting can be morphological and petro-chemical as well. This starts with undifferentiated rocks such as flood basalts or trapps as of low-K tholeiites, and shift to evolved terms such as tephrites, nephelinites, phonolites, hawaiites, mugearites, benmoreites, and trachytes [4] [6] [7] [11] [18] [20] [23] [25] [44] [63] [64]. The rifting advancement correlates with the petrography of volcanic rocks wherein early rifting in the Nyiragongo volcano started with relatively undifferentiated tholeiites, basanites and then with the evolution of rifting relay relatively high potassic and differentiated fooidic rocks. The tectonic style and stress regime (transtensional constraints) may have a control of the magma petrochemistry such as in the case of the extreme alkaline and carbonatite magmas that occur often along transverse faults that crosscut the main axial rift [28] [67] [68] [69] [70].

The fractional crystallization and crustal contamination contribute on large varieties of rock chemistry and petrography [71]-[76]. In practical, the fractional crystallization occurred when from the initially formed melt, crystallize phenocrysts that separate from the melt and constitute rocks that are petrographically and chemically different from the remained melt [75] [76]. In the western branch of the EARS, the magma differentiation and fractionation are perceived through the whole-rock composition diversities and SMIs compositions; where a decrease in MgO, CaO and an increase in alkali sum ($K_2O + Na_2O$), SiO_2 , characterize the evolution from primary to evolved melts from which rocks are formed (**Figure 12**).

The Nyiragongo 2002 SMIs revealed a picritic composition of melt that was more likely trapped during the early crystallization of clinopyroxene (augite);

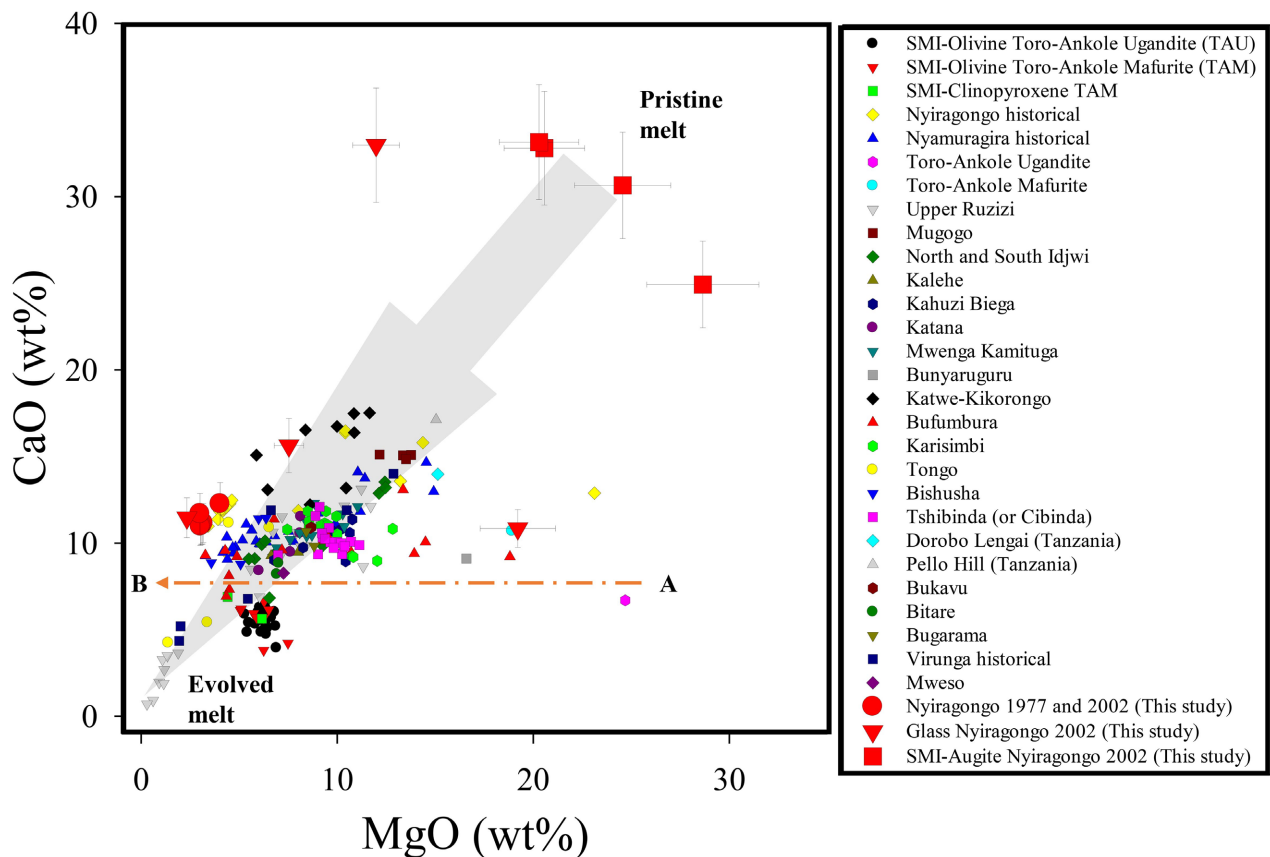


Figure 12. CaO versus MgO diagram showing silicate melt inclusions and whole-rock compositions of Nyiragongo 1977 and 2002 lavas and compiled volcanic rocks from the East African rift system western branch. Nyiragongo SMIs (red square symbols), defined as more likely primary melt having > 18 wt% MgO, and CaO above 20 wt% compared to the evolved Toro-Ankole nephelinitic melt where the CaO remained below 10 wt%. The orange and grey arrows show the evolution or differentiation of the magma from pristine to evolved melts. A and B are used as reference points to show the evolution. Data of silicate melt inclusions, glassy matrix and lavas were expressed as average \pm standard deviation. (Abbreviations: SMI = silicate melt inclusion).

and this, suggests that the magma would originate at least from the magmatic chamber R3 or below, and transported on the surface by the slant of volcanic activities (Figure 14(a)), [4] [7].

The Nd-Sm, Sr-Rb, He and Th isotopes suggested a bulk earth or a primitive component as of the mixing between enriched mantle EMI and depleted MORB; and high ratios of $^{208}\text{Pb}/^{204}\text{Pb}$, $^{207}\text{Pb}/^{204}\text{Pb}$ suggested an enriched mantle EMII contribution and phlogopite bearing source and carbonate metasomatism [4] [5]. Additionally, the Ra deficit in the Mugogo volcanic rocks suggested a phlogopite and carbonate melt involvements [36]. The Nyiragongo 1977 and 2002 high Rb/Sr and relatively low Zr/Nb, Ba/Rb ratios suggest an amphibole-poor and phlogopite-rich bearing source of material (Figures 13(a)-(d)).

The Nyiragongo plumbing system was structured in three levels of magma reservoirs including R3 (the intermittent reservoir connected to the crater lava lake), R2 (stratified/or not feeding reservoir located about 3 km below the crater), and R1 (parental magma chamber located about 15 km below the crater); and all of them are in the lithosphere part and alimanted by the rising deep

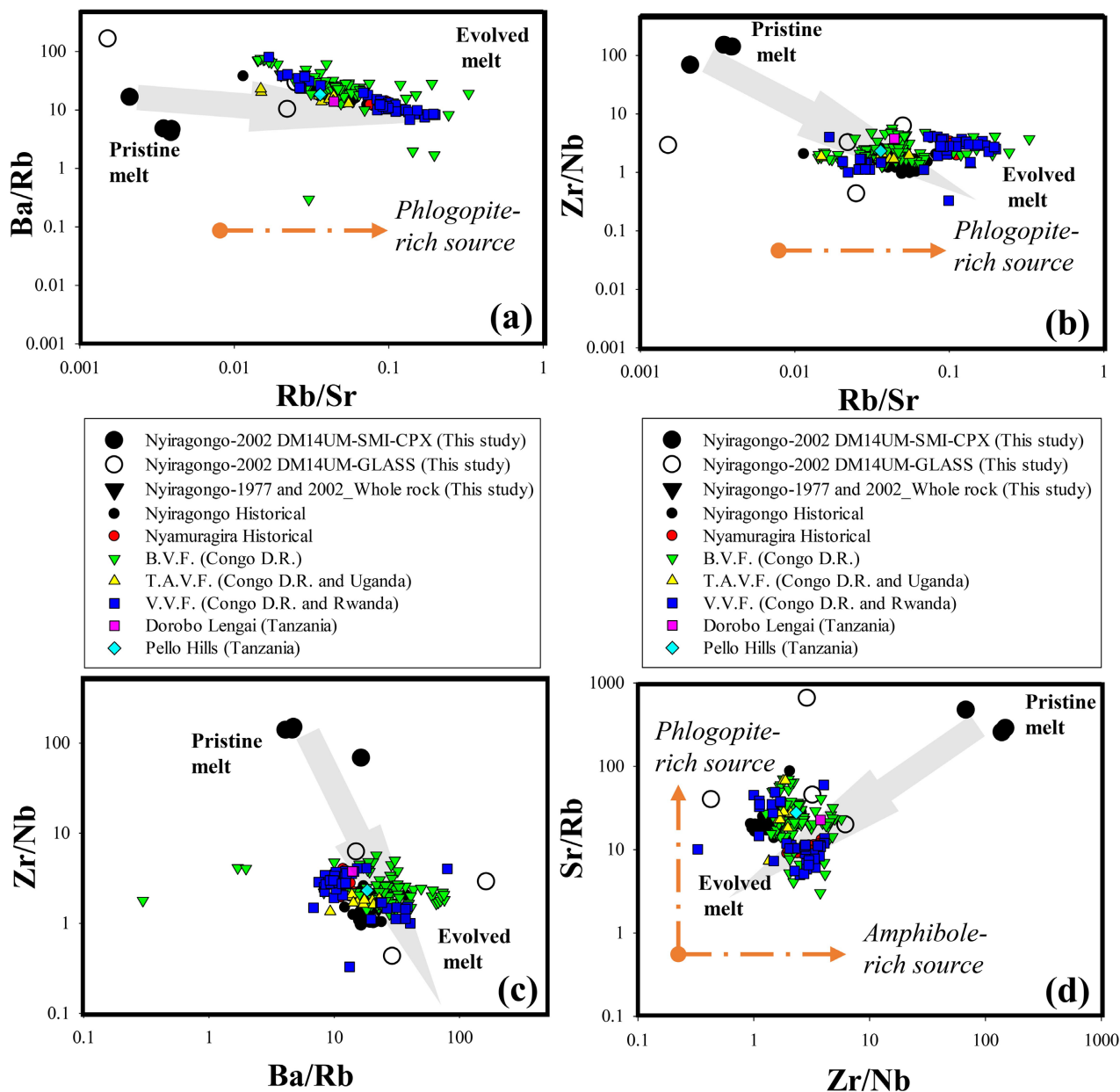


Figure 13. Plots of trace elements for compiled whole-rocks and silicate melt inclusions: (a) Ba/Rb versus Rb/Sr; (b) Zr/Nb versus Rb/Sr; (c) Zr/Nb versus Ba/Rb; and (d) Sr/Rb versus Zr/Nb. Orange arrows show trend field of material source type, grey arrows indicate the evolution melt from primary (picritic melt inclusion composition) to relatively evolved magmas. (*SMI* = silicate melt inclusion, *CPX* = clinopyroxene, *V.V.F.* = Virunga volcanic field, *B.V.F.* = Bukavu volcanic field, *T.A.V.F.* = Toro-Ankole volcanic field).

magmas from the asthenosphere (Figure 14(a)), [4] [7]. The chemical, petrographic, and mineralogical similarities of both 1977 and 2002 lavas suggest that they possibly originated from the same feeding reservoir. Unlike phenocrysts (augite, olivine) can crystallize anytime at any reservoir including R1, R2 and R3; and the chemistry of analyzed SMIs in augite suggests a pristine melt from the possibly R1.

In terms of rifting stages and morphology, starting from the rift initiation

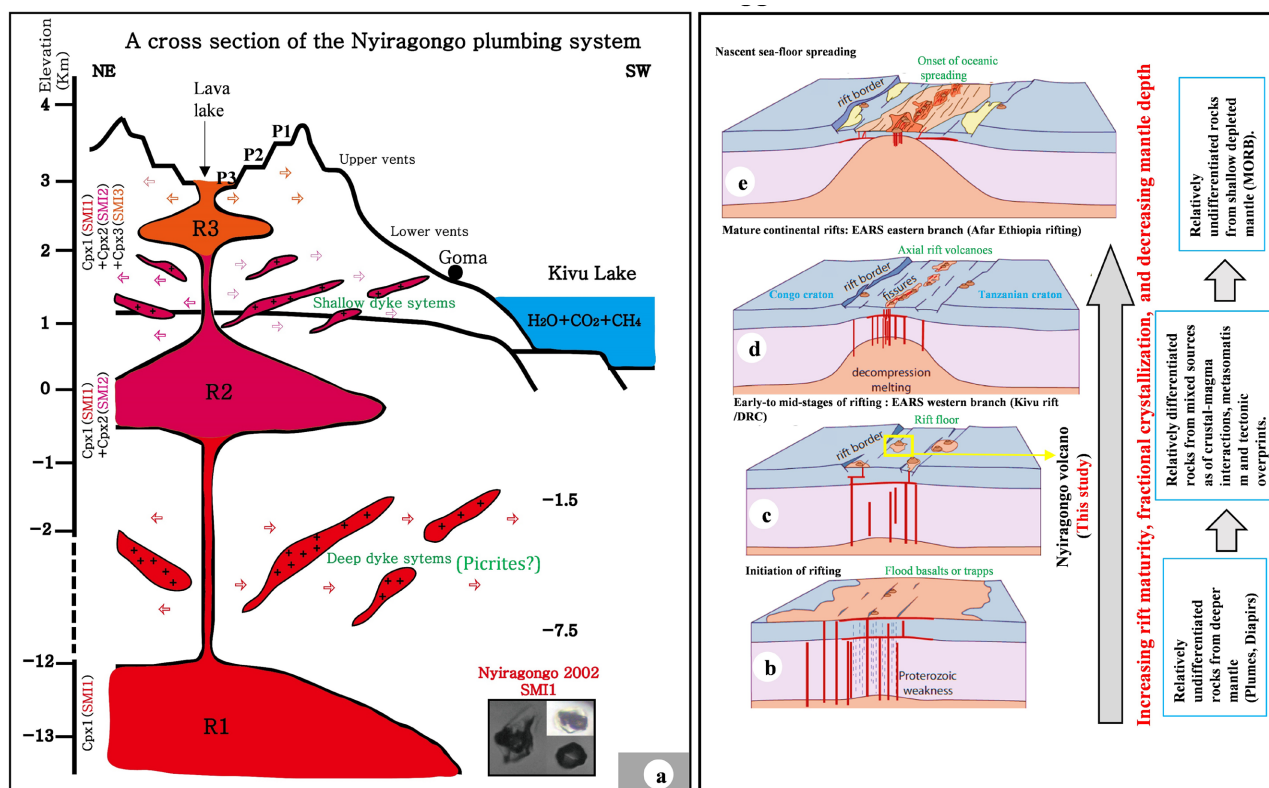


Figure 14. A suggested genetical model of the EARS: (a) A cross section of the Nyiragongo plumbing system showing various melt reservoirs, dyke systems and silicate melt inclusions possibly trapped minerals and areas; (b-e) Sketches illustrating the evolution of the rifting from the rift initiation to the Nascent Sea. Arrows in (a) show the spreading direction of the magma that form dyke systems and volcano shutter cones; and arrows in (b-e) Images are used to show the evolution stages of the rifting. (SMI = silicate melt inclusion, Cpx = clinopyroxene, P = volcano indoor platform, R = Magma primary and intermittent reservoirs or chambers). Modified after [7] [44].

stage to the nascent sea, the EARS especially in the western branch where is located the Nyiragongo volcano of this study can be considered as an intermediate rifting stage with arbored clusters of volcanoes in sparse grabens and rift valleys (Figures 14(b)-(e)), [4] [7].

5.3. SMI Analytical Problems, Difficulties, and Suggestions

The main problems and difficulties with analyses of silicate melt inclusions (SMIs) in the case of Nyiragongo 1977 and 2002 lavas are summarized to be related with operational stages and materials as follow:

1) The scarcity of phenocrysts in the lavas that potentially host SMIs; and therefore, lead to the non-abundance of analytical data. The bigger are data, the consistent are interpretation clues and attempts. To minimize the uncertainty, we have used statistical considerations as of average and standard deviation (Avg \pm 1std).

2) The size of SMIs influenced technically the analytical process because the laser minimum beam size was calibrated at 40 μ m for getting a relatively good signal, detection, and resolution especially for homogenous materials. The ma-

jority of SMIs in the Nyiragongo lava phenocrysts displayed small sizes (<30 μm); few melt inclusions exceeded 40 μm of diameter. Therefore, it was difficult in most cases to clearly distinguish and separate the SMI signal from that of host mineral (augite). Such signals were useless and declassified.

3) For the processing of LA-ICP-MS collected data of SMIs, we have used three (3) internal standards including Al, Si, and Mg depending on the fact that their signals are consistently and unambiguously observed; and in few cases, the use ratios of elements/internal standards (Al, Si, Mg) in final results. There is an urgent need to develop a standard reference material especially for the chemical microanalyses of SMIs.

6. Conclusions

We studied petrographic and geochemical characteristics of the Nyiragongo 1977 and 2002 lavas, and explored the possibility of tracing back the pristine and evolved melt compositions of the Nyiragongo volcano lavas 2002 in the western branch of EARS in the Democratic Republic of Congo through the combination of silicate melt inclusions (SMIs) for likely the first time, and regular petrographic and geochemical approaches. Noticeable findings are summarized below:

1) The Nyiragongo 1977 and 2002 lavas are silica undersaturated rocks as of melilite-nephelinites, texturally microlitic to sub porphyritic, and the mineralogical composition consisted of olivine, clinopyroxene (augite), phlogopite, melilite, and magnetite and rare plagioclases.

2) The whole-rock geochemical compositions of evolved Nyiragongo 1977 and 2002 lavas are barely distinguishable and showed low concentrations of SiO_2 (38.40 - 39.52 wt%) and MgO (3.10 - 4.01 wt%), relatively high concentrations of FeO (13.76 - 14.10 wt%), Al_2O_3 (15.01 - 16.48 wt%), CaO (11.00 - 12.29 wt%) and $\text{Na}_2\text{O} + \text{K}_2\text{O}$ (10.34 - 11.85 wt%).

3) LA-ICP-MS on SMIs hosted in augite showed a pristine melt as of picrite or picro basaltic composition that is poor in SiO_2 (31.14 - 32.26 wt%), FeO (2.19 - 2.79 wt%), Al_2O_3 (8.01 - 9.57 wt%), and $\text{Na}_2\text{O} + \text{K}_2\text{O}$ (2.34 - 3.05 wt%); while enriched in MgO (20.27 - 28.63 wt%), and CaO (24.95 - 33.17 wt%); suggesting a pristine melt from the reservoir R1.

4) A Raman spectroscopy on silicate melt inclusions showed the presence of gas species and sulfide metals such as carbon dioxide (CO_2), methane (CH_4), water (H_2O), sulfur dioxide (SO_2), anhydrate (CaSO_4), and chalcopyrite (CuFeS_2), and possibly pyrite (FeS_2) and magnetite (Fe_3O_4).

5) REE chondrite-normalized patterns were relatively similar in trends for lavas (1977 and 2002) and SMIs, even though the later showed lower concentrations; the sum ΣREE is respectively 712 - 799 and 43 - 119 ppm.

6) The contracted multi-element REE patterns showed a W-feature that characterizes most volcanic rocks from the EARS western branch, except for SMIs.

7) High Rb/Sr, and low Ba/Rb, Zr/Nb and Sm/Hf ratios of the Nyiragongo

1977 and 2002 lavas suggest a phlogopite-rich source of magma.

8) From the Nyiragongo 2002 SMI compositions, we suggest a possibility to find picritic rocks in the nearby magmatic chamber R1, especially in the deeper dyke system zones.

9) This study provides for the first time, melt inclusion evidence of pristine melt that is unambiguously distinguishable from evolved melts forming lavas at the ground surface, and this is consistent with magmatic evolutions that occurred in the western branch of the EARS in general, and the Nyiragongo volcano in particular. We can still expect for several decades to come that those volcanic eruptions of the Nyiragongo will release abundant liquid products (lava flows), and minor gas and solid (ash, falls, pyroclastic flows) products.

Recommendations

We suggest on basis of the present and previous studies on the Mt. Nyiragongo, the followings recommendations:

1) The results of this study and those of the previous researches on the Mt. Nyiragongo should be used for integrated prediction tools and methods of the future Nyiragongo volcanic eruptions, and save the lives of millions of people living in the vicinity of the volcano edifice.

2) We also recommend the government of DRC and any private investor to start as soon as possible the exploitation of the dry gas (methane, carbon dioxide) in the Kivu Lake to minimize hazard risks related to magma and flammables dry gas and susceptible to cause explosions and environment damages.

3) We finally suggest to use huge spilled volumes of lavas from volcanoes of the EARS (Nyiragongo, Nyamuragira and others volcanoes) as building materials.

Author Contributions

The Conception of the project, D.K.M.; field works and sampling, D.K.M.; petrographic and geochemical analyses (EPMA, LA-ICPMS, Raman spectroscopy, SEM-EDS, XRF, and petrographic microscopy), D.K.M.; data validation and curation, D.K.M.; writing—original draft preparation, D.K.M.; writing—review, editing, D.K.M.; supervision, D.K.M.; funding acquisition, D.K.M.

Funding

The present study received financial support from the National Institute for International Education and Development (NIIED-2020, grant number NIIED-200807-0012) in the Republic of Korea (D.K.M.); Bringmann and Kroëner Foundation (2020, grant number BEBUC-2015) in DRC (D.K.M).

Data Availability Statement

Data will be available at <https://orcid.org/0009-0001-9552-5250>, and <https://sciprofiles.com/projects/user/list/2877918>.

Acknowledgements

We kindly acknowledge Gerhard Bringmann, Mudogo Virima, Karine Ndjoko Ioset, Sangki Kwon, Jung Hun Seo, Insung Lee, Makutu Ma-Ngwayaya Adalbert, Kanika Mayena Thomas, and Kabonwa Janvier for constructive discussions, advice, and fruitful remarks on the achievements of this study. Thanks to Junhee Lee, TongHa Lee, Yevgeniya Kim, Yuri Choi, Hahyeon Park, Yechan Jeon, Ivan Bongwe and Dedel Milikwini for the material and sample preparations. Thanks to Dorothe Mamanongo Mapeto, Julie Idiamashi, Alexis Ingungu, Lele Marcelin, Noella Mukanyimi, Mipangu Joseph, and Ndala Yvan for their supports during the outcrop in DRC.

Conflicts of Interest

The author declares no conflict of interest related to this study.

References

- [1] Auchapt, A., Dupuy, C., Dostal, J. and Kanika, M. (1987) Geochemistry and Petrogenesis of Rift-Related Volcanic Rocks from South Kivu (Zaire). *Journal of Volcanology and Geothermal Research*, **31**, 33-46. [https://doi.org/10.1016/0377-0273\(87\)90004-7](https://doi.org/10.1016/0377-0273(87)90004-7)
- [2] Kampunzu, A.B., Sebagenzi, M.N., Caron, J.P.H. and Vellutini, P. (1982) Comparaison petrochimique entre les laves du champ Sud-Kivu (Bukavu) et Nord-Kivu (Virunga), Zaire. *Annale de la Société Géologique de Belgique*, **105**, 25-29.
- [3] Kampunzu, A.B., Bonhomme, M.G. and Kanika, M. (1998) Geochronology of Volcanic Rocks and Evolution of the Cenozoic Western Branch of the East African Rift System. *Journal of African Earth Sciences*, **26**, 441-461. [https://doi.org/10.1016/S0899-5362\(98\)00025-6](https://doi.org/10.1016/S0899-5362(98)00025-6)
- [4] Chakrabarti, R., Basu, A.R., Santo, A.P., Tedesco, D. and Vaselli, O. (2009) Isotopic and Geochemical Evidence for a Heterogeneous Mantle Plume Origin of the Virunga Volcanics, Western Rift, East African Rift System. *Chemical Geology*, **259**, 273-289. <https://doi.org/10.1016/j.chemgeo.2008.11.010>
- [5] Chakrabarti, R., Sims, K.W.W., Basu, A.R., Reagan, M. and Durieux, J. (2009) Timescales of Magmatic Processes and Eruption Ages of the Nyiragongo Volcanics from ^{238}U - ^{230}Th - ^{226}Ra - ^{210}Pb Disequilibria. *Earth and Planetary Science Letters*, **288**, 149-157. <https://doi.org/10.1016/j.epsl.2009.09.017>
- [6] Pouclet, A., Bellon, H. and Bram, K. (2016) The Cenozoic Volcanism in the Kivu Rift: Assessment of the Tectonic Setting, Geochemistry, and Geochronology of the Volcanic Activity in the South-Kivu and Virunga Regions. *Journal of African Earth Sciences*, **121**, 219-246. <https://doi.org/10.1016/j.jafrearsci.2016.05.026>
- [7] Pouclet, A. and Bram, K. (2021) Nyiragongo and Nyamuragira: A Review of Volcanic Activity in the Kivu Rift, Western Branch of the East African Rift System. *Bulletin of Volcanology*, **83**, Article No. 10. <https://doi.org/10.1007/s00445-021-01435-6>
- [8] Ongendangenda, T.A. (2020) Volcanologie de la chaîne des Virunga: Échos des profondeurs magmatiques. *Volcanologie de la chaîne des Virunga*, 1-308.
- [9] Komorowski, J.-C., Tedesco, D., Kasereka, M., Allard, P., Papale, P., Vaselli, O., Durieux, J., Baxter, P., Halbwachs, M., Akumbe, M., Baluku, B., Briole, P., Ciraba, M.,

- Dupin, J.-C., Etoy, O., Garcin, D., Hamaguchi, H., Houlié, N., Kavotha, K.S., Lemarchand, A., Lockwood, J., Lukaya, N., Mavonga, J., DeMichele, M., Mpore, S., Mukambilwa, K., Munyololo, F., Newhall, C., Ruch, J., Yalire, M.A. and Wafula, M. (2002) The January 2002 Flank Eruption of Nyiragongo Volcano (Democratic Republic of Congo): Chronology, Evidence for Tectonic Rift Trigger and Impact of Lava Flows on the City of Goma. *Acta Vulcanologica*, **14-15**, 27-62.
- [10] Head, E., Lanzirotti, A., Newville, M. and Sutton, S. (2018) Vanadium, Sulfur, and Iron Valences in Melt Inclusions as a Window into Magmatic Processes: A Case Study at Nyamuragira Volcano, Africa. *Geochimica et Cosmochimica Acta*, **226**, 149-173. <https://doi.org/10.1016/j.gca.2018.01.033>
- [11] Minissale, S., Casalini, M., Cucciniello, C., Balagizi, C., Tedesco, D., Boudoire, G., Morra, V. and Melluso, L. (2022) The Geochemistry of Recent Nyamulagira and Nyiragongo Potassic Lavas, Virunga Volcanic Province, and Implications on the Enrichment Processes in the Mantle Lithosphere of the Tanzania-Congo Craton. *Lithos*, **420-421**, Article ID: 106696. <https://doi.org/10.1016/j.lithos.2022.106696>
- [12] Hamaguchi, H., Wafula, M., Kasereka, M. and Akumbi, M. (2002) Preliminary Report on Emergency Survey of Nyiragongo Eruption on January 17, 2002; V032-004. Research Centre for Prediction of Earthquake and Volcanic Eruptions, Tohoku University, Miyagi, 1-2.
- [13] Cas, R.A.F. (2022) The Centenary of IAVCEI 1919-2019 and Beyond: Origins and Evolution of the International Association of Volcanology and Chemistry of the Earth's Interior. *Bulletin of Volcanology*, **84**, Article No. 15. <https://doi.org/10.1007/s00445-021-01509-5>
- [14] Cas, R.A.F. (2019) IAVCEI: From Small Beginnings to a Vibrant International Association. *History of Geo Space Sciences*, **10**, 181-191. <https://doi.org/10.5194/hgss-10-181-2019>
- [15] Wauthier, C., Smets, B. and Keir, D. (2015) Diking-Induced Moderate-Magnitude Earthquakes on a Youthful Rift Border Fault: The 2002 Nyiragongo-Kalehe Sequence, D.R. Congo. *Geochemistry, Geophysics, Geosystems*, **16**, 4280-4291. <https://doi.org/10.1002/2015GC006110>
- [16] Durieux, J. (2002) Volcano Nyiragongo (D.R. Congo): Evolution of the Crater and Lava Lakes from the Discovery to the Present. *Acta Vulcanologica*, **14-15**, 137-144.
- [17] Smets, B., d'Oreye, N., Kervyn, M. and Kervyn, F. (2017) Gas Piston Activity of the Nyiragongo Lava Lake: First Insights from a Stereographic Time-Lapse Camera System. *Journal of African Earth Sciences*, **134**, 874-887. <https://doi.org/10.1016/j.jafrearsci.2016.04.010>
- [18] Minissale, S., Zanetti, A., Tedesco, D., Morra, V. and Melluso, L. (2019) The Petrology and Geochemistry of Nyiragongo Lavas of 2002, 2016, 1977 and 2017 AD, and the Trace Element Partitioning between Melilitite Glass and Melilite, Nepheline, Leucite, Clinopyroxene, Apatite, Olivine and Fe-Ti Oxides: A Unique Scenario. *Lithos*, **332-333**, 296-311. <https://doi.org/10.1016/j.lithos.2019.02.023>
- [19] Giordano, D., Polacci, M., Longo, A., Papale, P., Dingwell, D.B., Boschi, E. and Kasereka, M. (2007) Thermo-Rheological Magma Control on the Impact of Highly Fluid Lava Flows at Mt. Nyiragongo. *Geophysical Research Letters*, **34**, L06301. <https://doi.org/10.1029/2006GL028459>
- [20] Rogers, N., De Mulder, M. and Hawkesworth, C. (1992) An Enriched Mantle Source for Potassic Basanites: Evidence from Karisimbi Volcano, Virunga Volcanic Province, Rwanda. *Contributions to Mineralogy and Petrology*, **111**, 543-556. <https://doi.org/10.1007/BF00320908>

- [21] Aoki, K.I., Yoshida, T., Yusa, K.A. and Nakamura, Y. (1985) Petrology and Geochemistry of the Nyamuragira Volcano, Zaire. *Journal of Volcanology and Geothermal Research*, **25**, 1-28. [https://doi.org/10.1016/0377-0273\(85\)90002-2](https://doi.org/10.1016/0377-0273(85)90002-2)
- [22] Demant, A., Lestrade, P., Lubala, R.T., Kampunzu, A.B. and Durieux, J. (1994) Volcanological and Petrological Evolution of Nyiragongo Volcano, Virunga Volcanic Field, Zaire. *Bulletin of Volcanology*, **56**, 47-61. <https://doi.org/10.1007/BF00279728>
- [23] Pitcavage, E., Furman, T., Nelson, W.R., Kalegga, P.K. and Barifaijo, E. (2021) Petrogenesis of Primitive Lavas from the Toro Ankole and Virunga Volcanic Provinces: Metasomatic Mineralogy beneath East Africa's Western Rift. *Lithos*, **396-397**, 1-20.
- [24] Agama, B.I., Chazot, G.A. and Kamgang, P. (2022) Pure Forsterite in Nyiragongo Lavas: Evidence for Subsolvus Oxidation of Volcanic Rocks. *Acta Geochimica*, **41**, 12-23. <https://doi.org/10.1007/s11631-021-00513-y>
- [25] Morrison, A.A., Whittington, A., Smets, B., Kervyn, M. and Sehlke, A. (2020) The Rheology of Crystallizing Basaltic Lavas from Nyiragongo and Nyamuragira Volcanoes, DRC. *Volcanica*, **3**, 1-28. <https://doi.org/10.30909/vol.03.01.0128>
- [26] Wurman (2022) Mount Nyiragongo 2002. Global Volcanism Program, Smithsonian Institution, Washington DC, 1-8.
- [27] Venzke, E. (2017) Report on Nyiragongo (DR Congo). *Bulletin of the Global Volcanism Network*, **42**, 1-9. <https://doi.org/10.5479/si.GVP.BGVN201701-223030>
- [28] Kampunzu, A. and Popoff, M. (1991) Distribution of the Main Phanerozoic African Rifts and Associated Magmatism: Introductory Notes. In: Kampunzu, A.B. and Lubala, R.T., Eds., *Magmatism in Extensional Structural Settings*, Springer, Berlin, 2-10. https://doi.org/10.1007/978-3-642-73966-8_1
- [29] Sequer, G.W. (2009) Neotectonics of the East African Rift System: New Interpretations from Conjunctive Analysis of Field and Remotely Sensed Datasets in the Lake Magadi Area, Kenya. ITC, Enschede, 1-22.
- [30] Acocella, V., Faccenna, C., Funicello, R. and Rossetti, F. (1999) Sand-Box Modelling of Basement-Controlled Transfer Zones in Extensional Domains. *Terra Nova-Oxford*, **11**, 149-156. <https://doi.org/10.1046/j.1365-3121.1999.00238.x>
- [31] Olivotos, S., Niedermann, S., Flügel, T., Mouslopoulou, V., Merchel, S., Cotterill, F., Bookhagen, B., Gärtner, A., Rugel, G., Scharf, A., Nadeau, M.-J., Braucher, R. and Seiler, M. (2021) Quaternary Landscape Evolution in a Tectonically Active Rift Basin (Paleo-Lake Mweru, South-Central Africa). *Geomorphology*, **381**, Article ID: 107669. <https://doi.org/10.1016/j.geomorph.2021.107669>
- [32] Pitcavage, E. (2020) Geochemical Investigations of Continental Rift Magmatism: A Case Study in East Africa's Western Rift. Pennsylvania State University, State College.
- [33] Gurenko, A.A. and Sobolev, A.V. (2018) Can Orthopyroxene Be Present in the Source of Toro-Ankole, East African Rift, Kamafugites? *Journal of Petrology*, **59**, 1517-1550. <https://doi.org/10.1093/petrology/egy069>
- [34] Platz, T., Foley, S.F. and André, L. (2004) Low-Pressure Fractionation of the Nyiragongo Volcanic Rocks, Virunga Province, D.R. Congo. *Journal of Volcanology and Geothermal Research*, **136**, 269-295. <https://doi.org/10.1016/j.jvolgeores.2004.05.020>
- [35] Lustrino, M., Luciani, N. and Stagno, V. (2019) Fuzzy Petrology in the Origin of Carbonatitic/Pseudocarbonatitic Ca-Rich Ultrabasic Magma at Polino (Central Italy). *Scientific Reports*, **9**, Article No. 9212.

- <https://doi.org/10.1038/s41598-019-45471-x>
- [36] Condomines, M., Carpentier, M. and Ongendangenda, T. (2015) Extreme Radium Deficit in the 1957 AD Mugogo Lava (Virunga Volcanic Field, Africa): Its Bearing on Olivine-Melilitite Genesis. *Contributions to Mineralogy and Petrology*, **169**, Article No. 29. <https://doi.org/10.1007/s00410-015-1124-9>
- [37] Smets, B., Kervyn, M., d'Oreye, N. and Kervyn, F. (2015) Spatio-Temporal Dynamics of Eruptions in a Youthful Extensional Setting: Insights from Nyamulagira Volcano (D.R. Congo), in the Western Branch of the East African Rift. *Earth-Science Reviews*, **150**, 305-328. <https://doi.org/10.1016/j.earscirev.2015.08.008>
- [38] Smets, B., Tedesco, D., Kervyn, F., Kies, A., Vaselli, O. and Yalire, M.M. (2010) Dry Gas Vents ("Mazuku") in Goma Region (North-Kivu, Democratic Republic of Congo): Formation and Risk Assessment. *Journal of African Earth Sciences*, **58**, 787-798. <https://doi.org/10.1016/j.jafrearsci.2010.04.008>
- [39] Albino, F., Smets, B., d'Oreye, N. and Kervyn, F. (2015) High-Resolution TanDEM-X DEM: An Accurate Method to Estimate Lava Flow Volumes at Nyamulagira Volcano (D. R. Congo). *Journal of Geophysical Research: Solid Earth*, **120**, 4189-4207. <https://doi.org/10.1002/2015JB011988>
- [40] Sawyer, G.M., Carn, S.A., Tsanev, V.I., Oppenheimer, C. and Burton, M. (2008) Investigation into Magma Degassing at Nyiragongo Volcano, Democratic Republic of the Congo. *Geochemistry, Geophysics, Geosystems*, **9**, Q02017. <https://doi.org/10.1029/2007GC001829>
- [41] Vaselli, O., Tassi, F., Tedesco, D., Cuoco, E., Nisi, B. and Yalire, M.M. (2007) Environmental Impact of the Nyiragongo Volcanic Plume after the January 2002 Eruption. *Proceedings of the Active Volcanism and Continental Rifting*, Luxembourg, 19-21 November 2007, 1-11.
- [42] Ryerson, F., Weed, H. and Piwinski, A. (1988) Rheology of Subliquidus Magmas: 1. Picritic Compositions. *Journal of Geophysical Research: Solid Earth*, **93**, 3421-3436. <https://doi.org/10.1029/JB093iB04p03421>
- [43] Vigneresse, J.L., Barbey, P. and Cuney, M. (1996) Rheological Transitions during Partial Melting and Crystallization with Application to Felsic Magma Segregation and Transfer. *Journal of Petrology*, **37**, 1579-1600. <https://doi.org/10.1093/petrology/37.6.1579>
- [44] Biggs, J., Ayele, A., Fischer, T.P., Fontijn, K., Hutchison, W., Kazimoto, E., Whaler, K. and Wright, T.J. (2021) Volcanic Activity and Hazard in the East African Rift Zone. *Nature Communications*, **12**, Article No. 6881. <https://doi.org/10.1038/s41467-021-27166-y>
- [45] Barrière, J., d'Oreye, N., Oth, A., Theys, N., Mashagiro, N., Subira, J., Kervyn, F. and Smets, B. (2019) Seismicity and Outgassing Dynamics of Nyiragongo Volcano. *Earth and Planetary Science Letters*, **528**, Article ID: 115821. <https://doi.org/10.1016/j.epsl.2019.115821>
- [46] Smittarello, D., Smets, B., Barriere, J., Michellier, C., Oth, A., Shreve, T., Grandin, R., Theys, N., Brenot, H., Cayol, V., Allard, P., Caudron, C., Chevrel, O., Darchambeau, F., de Buyl, P., Delhay, L., Derauw, D., Ganci, G., Geirsson, H., Kamate Kaleghetso, E., Kambale Makundi, J., Kambale Nguomoja, I., Kasereka Mahinda, C., Kervyn, M., Kimanuka Ruriho, C., Le Mevel, H., Molendijk, S., Namur, O., Poppe, S., Schmid, M., Subira, J., Wauthier, C., Yalire, M., d'Oreye, N., Kervyn, F. and Syavulisembo Muhindo, A. (2022) Precursor-Free Eruption Triggered by Edifice Rupture at Nyiragongo Volcano. *Nature*, **609**, 83-88. <https://doi.org/10.1038/s41586-022-05047-8>

- [47] Putirka, K.D. (2008) Thermometers and Barometers for Volcanic Systems. *Reviews in Mineralogy and Geochemistry*, **69**, 61-120.
<https://doi.org/10.1038/s41586-022-05047-8>
- [48] Mallmann, G. and O'Neill, H.S.C. (2013) Calibration of an Empirical Thermometer and Oxybarometer Based on the Partitioning of Sc, Y and V between Olivine and Silicate Melt. *Journal of Petrology*, **54**, 933-949.
<https://doi.org/10.1093/petrology/egt001>
- [49] Arato, R. and Audetat, A. (2017) Experimental Calibration of a New Oxybarometer for Silicic Magmas Based on Vanadium Partitioning between Magnetite and Silicate Melt. *Geochimica et Cosmochimica Acta*, **209**, 284-295.
<https://doi.org/10.1016/j.gca.2017.04.020>
- [50] Arato, R. and Audetat, A. (2017) Vanadium Magnetite-Melt Oxybarometry of Natural, Silicic Magmas: A Comparison of Various Oxybarometers and Thermometers. *Contributions to Mineralogy and Petrology*, **172**, Article No. 52.
<https://doi.org/10.1007/s00410-017-1369-6>
- [51] Arato, R. and Audetat, A. (2017) FeTiMM—A New Oxybarometer for Mafic to Felsic Magmas. *Geochemical Perspectives Letters*, **5**, 19-23.
<https://doi.org/10.7185/geochemlet.1740>
- [52] Neal, C.A., Brantley, S., Antolik, L., Babb, J., Burgess, M., Calles, K., Cappos, M., Chang, J., Conway, S. and Desmither, L. (2019) The 2018 Rift Eruption and Summit Collapse of Kilauea Volcano. *Science*, **363**, 367-374.
<https://doi.org/10.1126/science.aav7046>
- [53] Tang, Y., Tong, D.Q., Yang, K., Lee, P., Baker, B., Crawford, A., Luke, W., Stein, A., Campbell, P.C. and Ring, A. (2020) Air Quality Impacts of the 2018 Mt. Kilauea Volcano Eruption in Hawaii: A Regional Chemical Transport Model STUDY with satellite-Constrained Emissions. *Atmospheric Environment*, **237**, Article ID: 117648.
<https://doi.org/10.1016/j.atmosenv.2020.117648>
- [54] Anderson, K.R., Johanson, I.A., Patrick, M.R., Gu, M., Segall, P., Poland, M.P., Montgomery-Brown, E.K. and Miklius, A. (2019) Magma Reservoir Failure and the Onset of Caldera Collapse at Kilauea Volcano in 2018. *Science*, **366**, Article ID: 117648. <https://doi.org/10.1016/j.atmosenv.2020.117648>
- [55] Patrick, M.R., Dietterich, H.R., Lyons, J.J., Diefenbach, A.K., Parcheta, C. anderson, K.R., Namiki, A., Sumita, I., Shiro, B. and Kauahikaua, J.P. (2019) Cyclic Lava Effusion during the 2018 Eruption of Kilauea Volcano. *Science*, **366**, eaay9070.
<https://doi.org/10.1126/science.aay9070>
- [56] Whitty, R.C., Ilyinskaya, E., Mason, E., Wieser, P.E., Liu, E.J., Schmidt, A., Roberts, T., Pfeffer, M.A., Brooks, B. and Mather, T.A. (2020) Spatial and Temporal Variations in SO₂ and PM_{2.5} Levels around Kilauea Volcano, Hawai'i during 2007-2018. *Frontiers in Earth Science*, **8**, Article No. 36.
- [57] Garcia, M.O. (2002) Submarine Picritic Basalts from Koolau Volcano, Hawaii: Implications for Parental Magma Compositions and Mantle Source. *Geophysical Monograph-American Geophysical Union*, **128**, 391-402.
<https://doi.org/10.1029/GM128p0391>
- [58] Robertson, K., Simon, A., Pettke, T., Smith, E., Selyangin, O., Kiryukhin, A., Mulcahy, S. and Walker, J. (2013) Melt Inclusion Evidence for Magma Evolution at Mutnovsky Volcano, Kamchatka. *Geofluids*, **13**, 421-439.
<https://doi.org/10.1111/gfl.12060>
- [59] Jennings, E.S., Gibson, S.A., Maclennan, J. and Heinonen, J.S. (2017) Deep Mixing of Mantle Melts beneath Continental Flood Basalt Provinces: Constraints from Oli-

- vine-Hosted Melt Inclusions in Primitive Magmas. *Geochimica et Cosmochimica Acta*, **196**, 36-57. <https://doi.org/10.1016/j.gca.2016.09.015>
- [60] Venugopal, S., Schiavi, F., Moune, S., Bolfan-Casanova, N., Druitt, T. and Williams-Jones, G. (2020) Melt Inclusion Vapour Bubbles: The Hidden Reservoir for Major and Volatile Elements. *Scientific Reports*, **10**, Article No. 9034. <https://doi.org/10.1038/s41598-020-65226-3>
- [61] Cannatelli, C., Doherty, A.L., Esposito, R., Lima, A. and De Vivo, B. (2016) Understanding a Volcano through a Droplet: A Melt Inclusion Approach. *Journal of Geochemical Exploration*, **171**, 4-19. <https://doi.org/10.1016/j.gexplo.2015.10.003>
- [62] Abersteiner, A., Kamenetsky, V.S., Goemann, K., Golovin, A.V., Sharygin, I.S., Pearson, D.G., Kamenetsky, M. and Gornova, M.A. (2019) Polymineralic Inclusions in Kimberlite-Hosted Megacrysts: Implications for Kimberlite Melt Evolution. *Lithos*, **336-337**, 310-325. <https://doi.org/10.1016/j.lithos.2019.04.004>
- [63] Ashwal, L.D., Ziegler, A., Glynn, S., Truebody, T.A. and Bolhar, R. (2021) Sr-Enriched Glassy Picrites from Karoo Large Igneous Province Are Evolved, Not Primitive Magmatic Rocks. *South African Journal of Geology*, **2**, 1-5. <https://doi.org/10.1002/essoar.10503697.1>
- [64] Ashwal, L.D. (2021) Sub-Lithospheric Mantle Sources for Overlapping Southern African Large Igneous Provinces. *South African Journal of Geology*, **124**, 421-442. <https://doi.org/10.1002/essoar.10503697.1>
- [65] Jourdan, F., Bertrand, H., Schärer, U., Blichert-Toft, J., Féraud, G. and Kampunzu, A.B. (2007) Major and Trace Element and Sr, Nd, Hf, and Pb Isotope Compositions of the Karoo Large Igneous Province, Botswana-Zimbabwe: Lithosphere vs Mantle Plume Contribution. *Journal of Petrology*, **48**, 1043-1077. <https://doi.org/10.1093/petrology/egm010>
- [66] Harris, C., le Roux, P., Cochrane, R., Martin, L., Duncan, A.R., Marsh, J.S., le Roex, A.P. and Class, C. (2015) The Oxygen Isotope Composition of Karoo and Etendeka Picrites: High $\delta^{18}\text{O}$ Mantle or Crustal Contamination? *Contributions to Mineralogy and Petrology*, **170**, Article No. 8. <https://doi.org/10.1007/s00410-015-1164-1>
- [67] Harris, P., Clifford, T. and Gass, I. (1970) African Magmatism and Tectonics. Oliver and Boyd Publisher, London, 419-437.
- [68] Kumarapeli, P. (1985) Vestiges of Lapetan Rifting in the Craton West of the Northern Appalachians. *Geoscience Canada*, **12**, 54-59.
- [69] Nasir, S. and Klemd, R. (1998) New Carbonatite Occurrences along the Hatta Transform Fault Zone (Northern Oman Mountains, United Arab Emirates). *Journal of African Earth Sciences*, **27**, 3-10. [https://doi.org/10.1016/S0899-5362\(98\)00042-6](https://doi.org/10.1016/S0899-5362(98)00042-6)
- [70] Baer, G., Hamiel, Y., Shamir, G. and Nof, R. (2008) Evolution of a Magma-Driven Earthquake Swarm and Triggering of the Nearby Oldoinyo Lengai Eruption, as Resolved by InSAR, Ground Observations and Elastic Modeling, East African Rift, 2007. *Earth and Planetary Science Letters*, **272**, 339-352. <https://doi.org/10.1016/j.epsl.2008.04.052>
- [71] Hickey-Vargas, R., Roa, H.M., Escobar, L.L. and Frey, F.A. (1989) Geochemical Variations in Andean Basaltic and Silicic Lavas from the Villarrica-Lanin Volcanic Chain (39.5 S): An Evaluation of Source Heterogeneity, Fractional Crystallization and Crustal Assimilation. *Contributions to Mineralogy and Petrology*, **103**, 361-386. <https://doi.org/10.1007/BF00402922>
- [72] Condie, K.C. (1985) Secular Variation in the Composition of Basalts: An Index to Mantle Evolution. *Journal of Petrology*, **26**, 545-563.

- <https://doi.org/10.1093/petrology/26.3.545>
- [73] Harris, C., Smith, H.S. and le Roex, A.P. (2000) Oxygen Isotope Composition of Phenocrysts from Tristan da Cunha and Gough Island Lavas: Variation with Fractional Crystallization and Evidence for Assimilation. *Contributions to Mineralogy and Petrology*, **138**, 164-175. <https://doi.org/10.1007/s004100050015>
- [74] Davies, G. and Macdonald, R. (1987) Crustal Influences in the Petrogenesis of the Naivasha Basalt—Comendite Complex: Combined Trace Element and Sr-Nd-Pb Isotope Constraints. *Journal of Petrology*, **28**, 1009-1031. <https://doi.org/10.1093/petrology/28.6.1009>
- [75] Pearce, J.A., Baker, P.E., Harvey, P.K. and Luff, I.W. (1995) Geochemical Evidence for Subduction Fluxes, Mantle Melting and Fractional Crystallization beneath the South Sandwich Island Arc. *Journal of Petrology*, **36**, 1073-1109. <https://doi.org/10.1093/petrology/36.4.1073>
- [76] Meen, J.K. (1990) Elevation of Potassium Content of Basaltic Magma by Fractional Crystallization: The Effect of Pressure. *Contributions to Mineralogy and Petrology*, **104**, 309-331. <https://doi.org/10.1007/BF00321487>